HHS Public Access

Author manuscript

Nat Aging. Author manuscript; available in PMC 2023 November 01.

Published in final edited form as:

Nat Aging. 2023 May ; 3(5): 600–616. doi:10.1038/s43587-023-00399-w.

CISH impairs lysosomal function in activated T cells resulting in mitochondrial DNA release and inflammaging

Jun Jin[1,2,3,5,*], **Yunmei Mu**[2,5], **Huimin Zhang**[2,3], **Ines Sturmlechner**[2], **Chenyao Wang**[4], **Rohit R. Jadhav**[2,3], **Qiong Xia**[3], **Cornelia M. Weyand**[2,3,4], **Jorg J. Goronzy**[2,3,4,*]

[1]Multiscale Research Institute of Complex Systems, Fudan University, Shanghai, China

[2]Department of Immunology, Mayo Clinic, Rochester, MN, USA.

[3]Department of Medicine, Stanford University, Stanford, CA, USA.

[4]Department of Medicine, Division of Rheumatology, Mayo Clinic, Rochester, MN, USA

[5]JJ and YM contributed equally

Abstract

Chronic systemic inflammation is one of the hallmarks of the aging immune system. Here we show that activated T cells from older adults contribute to inflammaging by releasing mitochondrial DNA (mtDNA) into their environment due to an increased expression of the Cytokine Inducible SH2-containing protein (CISH). CISH targets ATP6V1A, an essential component of the proton pump V-ATPase, for proteasomal degradation, thereby impairing lysosomal function. Impaired lysosomal activity caused intracellular accumulation of multivesicular bodies and amphisomes and the export of their cargos, including mtDNA. *CISH* silencing in T cells from older adults restored lysosomal activity and prevented amphisomal release. In antigen-specific responses in vivo, CISH-deficient $CD4^+$ T cells released less mtDNA and induced less inflammatory cytokines. Attenuating CISH expression may present a promising strategy to reduce inflammation in an immune response of older individuals.

Keywords

Lysosome; amphisome; mitochondrial damage; circulating mtDNA; T cell aging; immunosenescence; inflammation

Introduction

Characteristic hallmarks of immune aging are a decline in adaptive immunity[1, 2, 3], clinically manifesting as increased susceptibility to infections and decreased efficacy of vaccinations, in combination with inflammaging, a low-grade systemic inflammatory state that contributes

*Correspondence: goronzy.jorg@mayo.edu or jun_jin@fudan.edu.cn.

Author contributions: J.J., Y.M., C.M.W., and J.J.G. designed the study. J.J., Y.M., H.Z., I.S., C.W., and Q.X. performed the experiments. R.J. performed the computational analysis. J.J., Y.M., C.M.W., and J.J.G. analyzed and interpreted the data. J.J., Y.M. and J.J.G. wrote the manuscript with all authors providing feedback.

Competing interests: The authors declare no competing interests.

to widespread tissue dysfunction, frailty and premature death[4, 5]. Inflammatory mediators are produced by a variety of mechanisms, some of which are controlled by T cells, suggesting a causal relationship between changes in the adaptive immune system and inflammaging. The aged T cell repertoire is shaped by an accumulation of T effector cell populations that produce pro-inflammatory cytokines, in part in response to chronic viral infections such as Epstein-Barr virus (EBV) and Cytomegalovirus (CMV)[6]. Some T cell population, such as terminally differentiated effector memory (TEMRA) cells have acquired innate cell-like properties, enabling them to respond to stimuli other than antigen to produce interferon (IFN)-γ and other cytokines[7, 8, 9].

This pro-inflammatory T cell state is not limited to established immunity and effector memory cells. Naïve T cells from older adults have a propensity to differentiate into effector T cells due to sustained mTORC1 pathway activation and induction of transcription factor networks dominated by BATF, BLIMP1 and RUNX rather than TCF1[10, 11]. Activation of DNA damage responses in T cells from older adults due to telomere shortening, replication stress and loss of DNA repair molecules further contribute to this inflammatory state[12, 13, 14, 15]. Most but not all of these T cell-derived effector molecules are cytokines. A recent study has identified granzyme K, produced by a $CD8^+$ T cell population in older mice and human adults, as an inducer of inflammatory mediators in senescent cells, also called senescence-associated secretory pattern or SASP[16].

In addition to the baseline steady state of inflammatory mediator production in the absence of obvious exogenous stimuli, inflammaging also manifests as excess inflammation in an acute immune response. When occurring in the context of vaccination, it is frequently associated with reduced efficacy in older adults[17, 18, 19, 20]; conversely, inhibition of inflammation can improve vaccine efficacy[21]. Excess inflammation occurring in the context of an acute infection in older individuals can result from increased viral load due to reduced or delayed T cell responses but can also reflect an active mechanism by the responding T cell population. In general, the increased inflammatory response is not beneficial for the infected host but is associated with excessive tissue injury. As a recent prime example, hyperinflammation can be induced by SARS-CoV-2 infections and is then positively correlated with disease severity and death, including in older adults[22, 23]. The underlying mechanisms have been unresolved although it is remarkable that the disease is associated with severe lymphopenia, reminiscent of the strongly inflammatory lymphocyte pyroptosis in HIV patients[24]. T cell pyroptosis due to mtDNA-induced inflammasome activation also contributes to the inflammation in rheumatoid arthritis[25]. In addition, T cell responses from older adults have been shown to be associated with increased secretion of granzyme B-containing exosomes, increased DNA damage responses and increased cell death from purinergic signals that all may contribute to inflammation[13, 26, 27].

Here, we describe that activated $CD4^+$ T cells from older adults release mtDNA that is known as a powerful inflammatory mediator. Activation of naïve $CD4^+$ T cells from older adults resulted in the increased expression of CISH due to failed repressive action of TCF1. CISH facilitated proteasomal degradation of the V-type proton ATPase catalytic subunit A (ATP6V1A), a component of the vacuolar ATPase that mediates acidification of lysosomes. Reduced ATP6V1A protein prevented lysosomal clearance of autophagosomes

and multivesicular bodies (MVBs), leading to intracellular amphisome accumulation and subsequent extracellular release of their cargo. In murine infection and immunization models, *Cish* silencing in antigen-specific T cells reduced serum mtDNA and inflammatory serum cytokines, while improving antibody production. In conclusion, targeting CISH expression in T cell responses is a promising strategy to reduce inflammaging and boost immunity in older individuals.

Results

Increased CISH expression in naïve T cells from older adults

mtDNA is appreciated as an important inflammatory mediator, mainly produced by innate immune cells but also other cell types upon activation and cellular stress. T cell activation is associated with extensive mitochondrial biogenesis and upregulation of oxidative phosphorylation. To screen for inflammatory mediators produced by activated T cells, we determined mtDNA in their supernatants. We found increased concentrations in cultures of activated naïve $CD4^+$ T cells from older compared to young adults (Fig. 1a), independent of gender (Extended Data Fig. 1a). Cytoplasmic mtDNA is degraded by DNase II, a lysosomal DNase[28]. Consistent with this clearance function of lysosomes, chloroquine (CQ) and bafilomycin A1 (Baf) promoted the release of mtDNA into the culture supernatants (Extended Data Fig. 1b). Lysosomal acidification (Extended Data Fig. 1c) and proteolytic activity (Fig 1b) were reduced in activated $CD4^+$ T cells from older compared to younger adults. To identify differentially expressed genes that could account for the lysosomal dysfunction, we reanalyzed previously published RNA-seq and ATAC-seq data of naïve $CD4^+$ T cells from young and old adults in the first 48 hours after activation. Cytoscape gene network analysis identified *CISH* as one of the top genes, multiple regulatory regions of which were more accessible, and the gene was more transcribed in cells from older individuals (Fig. 1c). CISH has been shown to be an important negative regulator of endolysosomal acidification[29]. Indeed, silencing of CISH in naïve $CD4^+$ T cells from older individuals reduced activation-induced mtDNA release (Fig 1d and Extended data Fig.1d). Kinetic analysis of the human naïve $CD4^+$ T cell transcriptome after stimulation showed an induction of *CISH* transcripts after activation that was more pronounced with older age (Fig. 1e). The age-associated differences in CISH expression persisted at least until day 5 after activation (Fig. 1f). They were also seen for naïve CD8 T cells but not for activated B cells (Extended Data Fig. 1e). Activated monocytes did not express CISH. Consistent with the transcriptomic data, protein expression of CISH increased after activation and was significantly higher in activated T cells from older adults as shown by immunoblotting and flow cytometry (Fig. 1g).

In exploring upstream regulators of CISH, we found that CISH is a target gene of TCF1 as suggested by transcriptome data (accession number PRJNA546023) comparing stem-like ($TCF1^+$) vs. exhausted ($TCF1^-$) mouse $CD8^+$ T cells (Fig. 1h)[30]. TCF1 declines upon T cell activation (Extended Data Figure 1f) and is significantly lower in activated T cells from older adults (Fig. 1i). Silencing of *TCF7* (encoding TCF1) in activated naïve $CD4^+$ T cells from young individuals promoted extracellular mtDNA release to the extent seen with older adults, suggesting that reduced TCF1 accounted for the age-associated increase

(Fig. 1j). Silencing of *TCF7* in activated naïve CD4$^+$ T cells from young adults reduced lysosomal acidification and proteolytic activities (Extended Data Fig. 1g), indicating that TCF1 prevents mtDNA release through regulating lysosomal activity. Stimulation of the WNT pathway by a GSK3 inhibitor resulting in increased TCF1 expression restored lysosomal acidification and lysosomal proteolytic activities and prevented mtDNA release by activated T cells from older adults (Extended Data Fig. 1h and i). Since GSK3 inhibition has broad effects aside upregulating WNT signaling and TCF1, we directly confirmed that *CISH* transcription is repressed by TCF1. We performed *TCF7* silencing in naïve CD4$^+$ T cells from young adults and found increased CISH transcript and protein expression (Fig. 1k-l). Conversely, forced overexpression of *TCF7* reduced CISH protein in activated T cells from older adults (Extended Data Fig.1j). Moreover, GSK3 inhibition reduced transcription (Fig. 1m) and protein of CISH (Fig. 1n).

CISH impairs lysosome function by promoting ATP6V1A degradation

To examine whether the increased CISH expression accounts for impaired lysosomal activities, we performed *CISH* silencing in naïve CD4$^+$ T cells from older adults and found increased lysosomal acidification and proteolytic activities (Fig. 2a). Silencing of *CISH* in T cells from young adults also improved lysosomal acidification but to a lesser extent (Extended Data Fig. 2a). In contrast, *CISH* overexpression in activated T cells from young adults reduced both, similar to direct silencing of *ATP6V1A* (Fig. 2b).

CISH has been reported as a scaffolding protein that promotes ubiquitination of bound proteins and their subsequent proteasomal degradation[31, 32]. Previous studies have found CISH to bind ATP6V1A, which is part of the V-ATPase multi-subunit complex that regulates lysosomal function and in particular luminal acidification[29]. We explored whether the effects of CISH on lysosomal function was due to regulating ATP6V1A protein levels and found that *CISH* silencing increased ATP6V1A protein expression (Fig. 2c). To determine whether CISH regulates proteasomal degradation of ATP6V1A, we inhibited proteasome activity with MG132. ATP6V1A protein levels increased in activated T cells from older adults after proteosome inhibition, but much less so in T cells from younger adults (Fig. 2d). Under MG132 treatment, *CISH* silencing no longer showed any effects on ATP6V1A protein levels (Fig. 2e), suggesting that CISH regulates ATP6V1A protein through the proteasome pathway. Immunoprecipitation of ATP6V1A from MG132-treated cells identified CISH complexed to ATP6V1A (Fig. 2e). Moreover, *CISH* silencing reduced ATP6V1A ubiquitination, suggesting that the CISH-ATP6V1A interaction facilitated ubiquitination (Fig. 2e). Confocal imaging confirmed colocalization of CISH and ATP6V1A in the cytoplasm (Extended Data Fig. 2b). ATP6V1A half-life in *CISH*-silenced naïve CD4$^+$ T cells was prolonged compared to control-silenced cells (Fig. 2f). Consistent with increased expression of *CISH*, day 3-activated naïve CD4$^+$ T cells from older adults had lower ATP6V1A protein as compared to young individuals (Fig. 2g). No age-associated change in proteasome activity was observed, excluding the possibility that housekeeping proteasomal activities contributed to age-related changes of ATP6V1A protein levels (Extended Data Fig. 2c). While silencing of *CISH* in T cells from older adults reduced mtDNA release (Fig. 1d), silencing of ATP6V1A in T cells from young adults promoted releasee (Fig. 2h and Extended Fig. 2d). Taken together, these data document that CISH

binds to ATP6V1A facilitating its ubiquitination and subsequent proteasomal degradation and thereby contributes to lysosome dysfunction with age.

CISH impairs autophagy in naïve T cells from older adults

The lysosome is a terminal degradation center for autophagy, and lysosomal dysfunction impairs autophagic flux[33, 34]. After activation, T cells from older adults that had increased CISH and lower ATP6VA1 had higher baseline of LC3B-II, an autophagosome marker that is degraded in lysosomes, while LC3B-I was not different (Fig. 3a and b). After adding Baf or CQ to inhibit lysosomal degradation, LC3B-II protein increased to the same level in T cells from young and older adults (Fig. 3a and b), consistent with an impaired lysosomal degradation of LC3B-II in T cells from older individuals. To directly determine autophagic flux, we lentivirally transduced naïve $CD4^+$ T cells from young and older adults with the RFP-LC3 or RFP-GFP-LC3 tandem fluorescent probes and determined the frequencies of fluorescent cells by cytometry. LC3 targets the probe to the autophagosome, the fluorescence of GFP is quenched when exposed to low pH while RFB is stable. Similar to LC3B-II, frequencies of RFP-fluorescinating cells were increased in T cells from older adults indicating reduced degradation (Fig. 3c). In studies with the RFP-GFP-LC3, the ratio of the acid-labile GFP to the more resistant RFP fluorescence was increased indicating reduced autophagic flux in activated T cells from older adults (Fig. 3c). Manipulation of CISH expression recapitulated age-associated changes of LC3B-II. As shown in Fig. 3d, overexpression of CISH increased LC3B-II baseline while not affecting LC3B-I or LC3B-II after CQ-treatment. Conversely, *CISH* silencing in T cells from older individuals reduced LC3B-II baseline consistent with improved autophagic flux (Fig. 3e). cGAS-Sting signaling was not involved in the CISH-induced impairment in autophagic flux. Treatment with the cGAS inhibitor G140 did not prevent the reduction of mtDNA release by *CISH* silencing (Fig. 3f).

CISH impairs the clearance of autophagosomes and autolysosomes

To explore morphological correlates of autophagic events, we performed transmission electron microscopy (TEM) to visualize and quantify autophagosomes and autolysosomes. Consistent with reduced autophagic flux, day 3-activated naïve $CD4^+$ T cells from older adults had significantly more autophagosomes and autolysosomes than those of young individuals (Fig. 4a). Reducing lysosomal activities in T cells from young individuals by either *ATP6V1A* silencing (Fig. 4a), *CISH* overexpression (Fig. 4b) or bafilomycin treatment (Fig. 4c) increased the numbers of autophagosomes and autolysosomes. In contrast, enhancing lysosomal activities in T cells from older adults by *CISH* silencing reduced their numbers (Fig. 4a) without that the number of lysosomes significantly increased (Extended Data Fig. 3). The accumulation of autophagic vacuoles-including autophagosomes was much more prominent on day 3 after activation than at the resting state of naïve $CD4^+$ T cells from older individuals that has been previously reported[35]. Taken together, these data indicate that excessive induction of *CISH* transcription in T cell responses from older adults impairs autophagic flux, leading to intracellular accumulation of autophagosomes and autolysosomes containing non-degraded cargo.

CISH induces MVB expansion in naïve CD4+ T cells

In addition to autophagosomes, MVBs are organelles that are joined to lysosomes for degradation of their cargo[36]. Due to reduced lysosomal activities, day 3-activated naïve $CD4^+$ T cells from older adults had increased MVBs compared to cells from young individuals (Fig. 5a). Again, MVB numbers could be modulated by regulating lysosomal activities. Enhancing lysosomal activities in T cells from older adults by *CISH* silencing reduced the numbers of MVBs. Conversely, inhibiting lysosomal activities in T cells from young individuals by *ATP6V1A* silencing increased their numbers (Fig. 5a). Single cell ATAC/RNA-seq (scMultiomics) data from a previous study comparing naïve $CD4^+$ T cells from young and older adults 18h after activation showed an enrichment for the endosomal vacuolar gene pathway in cells of older individuals that had high CISH expression (Fig. 5b). As previously reported, this cluster was enlarged in the older population[11]. Taken together, increased CISH expression in T cells from older individuals results in an expansion of the late endosomal compartment.

CISH impairs clearance of damaged mitochondria

TEM images showed higher frequencies of damaged mitochondria in activated T cells from older individuals compared to those from young adults (Fig. 6a). Again, these age-related changes depended on lysosomal activities as modulated by CISH. *CISH* silencing reduced the frequencies of damaged mitochondria in T cells from older adults. Conversely, *ATP6V1A* silencing increased their frequencies in T cells from young individuals (Fig. 6a). While we observed increased frequencies of damaged mitochondria in naïve $CD4^+$ T cell responses from older individuals, the total numbers of intracellular mitochondria were not affected by age (Fig. 6a). Moreover, levels of COX IV as determined by immunoblotting were not influenced by age suggesting no change in mitochondrial mass (Extended Fig. 4a). For a more quantitative assessment of mitochondrial damage, we used flow cytometry. Cell populations with damaged mitochondria can be identified as displaying lower mitochondrial membrane potential, in particular a population referred to as $TMRM^{lo}MtG^{hi}$ cells has been described that combine a low potential with increased mass[37]. We found that the frequencies of activated $CD4^+$ T cells with low membrane potential increased with age, including but not limited to $TMRM^{lo}MtG^{hi}$ cells (Fig. 6b and Extended Data Fig. 4b). These cells were small without evidence of apoptosis (Extended Fig. 4b). They had reduced TCF1 expression and higher CISH expression compared to the main population (Fig. 6c). Lysosensor staining and lysosomal proteolytic activity were reduced. TEM studies confirmed a higher frequency of damaged mitochondria in the sorted $TMRM^{lo}MtG^{hi}$ compared to the $TMRM^{hi}MtG^{hi}$ population while the total numbers of mitochondria per cells was not different (Fig. 6d). Consistent with our studies on age-associated lysosomal dysfunction, CISH expression was an upstream regulator of accumulation of damaged mitochondria. CISH silencing in day 3-activated naïve $CD4^+$ T cells from older individuals reduced the frequencies of the $TMRM^{lo}MtG^{hi}$ population to about the same frequencies as in young adults (Fig. 6b). Conversely, lysosome inhibition by *ATP6V1A* silencing or *CISH* overexpression increased the frequencies of the $TMRM^{lo}MtG^{hi}$ population in T cells from young individuals (Fig. 6e and f). Similar effects were observed for the $TMRM^{lo}MtG^{lo}$ population that were also enriched in older adults (Extended Fig. 4c) Taken together, these data document an

intracellular accumulation of damaged mitochondria in T cell responses from older adults that was caused by reduced lysosomal activities due to increased CISH expression.

CISH promotes amphisomal exocytosis of mitochondria

As described in Fig. 5, activated T cells from older adults have an expanded late endosomal compartment with accumulation of MVBs that are prone to release exosomes[26]. In addition to MVBs, T cells from older individuals had an abundance of endosomal vacuoles (Fig. 7a). Again, this age-related change is regulated by lysosomal activity. Enhancing lysosomal activities by *CISH* silencing in activated T cells from older individuals reduced endosomal vacuole numbers, whereas inhibiting lysosomal activities by *ATP6V1A* silencing in T cells from young adults increased their numbers (Fig. 7a). These endosomal vacuoles appeared to be distinct from regular MVBs. MVBs showed dozens of intraluminal vesicles (ILVs) with a size ranging from ~50 nm to ~100 nm inside the lumen that were released into the extracellular milieu as exosomes (Fig. 5a). The endosomal vacuoles contained autophagic cargo, double-bilayer membrane-structured autophagosome-like vesicles and damaged mitochondria in the lumen (Fig. 7b), suggesting that they represent amphisomes. Confocal imaging showed accumulation of structures with CD63/LC3B and CD63/COX IV colocalizing in activated T cells from older individuals, but not in *CISH*-silenced cells or in cells from young adults, indicating again the existence of mitochondria-containing amphisomes in activated T cells from older adults (Extended Data Fig. 5a and b). Frequencies of Annexin V^+ apoptotic cells were not different in the populations, excluding that amphisosme-containing cells were apoptotic (Extended Data Fig. 6a). Moreover, the amphisome-rich T cells from older adult did not display the electron morphology of apoptotic cells, such as condensed and fragmented chromatin and budding of apoptotic bodies (Extended Data Fig. 6b). Consistent with *CISH* expression being downstream of TCF1, silencing of *TCF7* in young adults promoted the intracellular accumulation of amphisomes (Extended Data Fig. 7). Taken together, these data documented the accumulation of damaged mitochondria-containing amphisomes in activated naïve $CD4^+$ T cells from older individuals due to increased CISH expression causing lysosomal dysfunction.

Studies of TEM images of T cells from older adults suggested the disposal of amphisome cargo into the extracellular space. Fig. 7c shows a cell where the luminal content (exosomes and damaged mitochondria) of an amphisome was not yet completely detached from the cell membrane; another amphisome appeared to be close to undergoing exocytosis. Other cells appeared to have completely released a cargo resembling that in amphisomes (Fig. 7d). In cross-sectional TEM analyses, we identified cells in different states that represented the sequence of events in amphisomal exocytosis: 1) mitophagy induction, 2) MVB and autophagosome contact and fusion, 3) amphisome formation and migration towards the plasma membrane, 4) amphisome and plasma membrane fusion, 5) amphisomal exocytosis of luminal mitochondria, 6) dispersing damaged mitochondria in the extracellular space (Fig. 7e). Taken together, these data document an amphisome-dependent release of damaged mitochondria that was higher in T cell responses from older individuals due to increased CISH expression and lysosomal dysfunction.

Cish silencing attenuates mtDNA-induced inflammation in vivo

To investigate whether CISH-dependent extracellular release of mtDNA causes inflammation in vivo, we used the LCMV infection mouse model. We retrovirally transduced SMARTA $CD4^+$ T cells with short hairpin RNA (shRNA) specific for *Cish* (sh*Cish*) or control shRNA (shCtrl) and transferred the cells into 5- to 8-week-old B6 mice followed by acute LCMV infection. Reduced CISH protein expression and increased lysosomal activities after *Cish* silencing were confirmed before adoptive transfer (Fig. 8a-c). At day 6 after LCMV infection, mice having received *Cish*-silenced SMARTA $CD4^+$ T cells had reduced serum mtDNA concentrations compared to mice with control-silenced cells (Fig. 8d). TEM images showed reduced numbers of amphisomes in *Cish*-silenced $CD4^+$ SMARTA cells compared to control cells (Fig. 8e), indicating that the reduced serum mtDNA levels were at least in part due to reduced amphisomal exocytosis. Consistent with reduced serum mtDNA levels, mice receiving *Cish*-silenced SMARTA $CD4^+$ T cells had lower inflammatory cytokine serum concentrations as well as lower cytokine transcripts in splenocytes compared to mice having received control-silenced cells (Fig. 8f and g). Virus clearance from spleen was not different in mice receiving wild-type or *Cish*-silenced SMARTA $CD4^+$ T cells (Extended Data Figure 8a). Also, no difference due to Cish silencing was seen for the differentiation of SMARTA T cells as shown for expression of CD69 and CD44 or TH1 and TFH markers (Extended Data Fig.8b-d). *Cish* silencing with a second shRNA reproduced the data (Extended Data Fig. 9), excluding off-targets effects.

To determine whether CISH dependent inflammation is seen in a non-infectious model, we used ovalbumin (OVA) immunization. We retrovirally transduced OT-II $CD4^+$ T cells with *Cish* or Ctrl shRNA and transferred the cells into 5- to 8-week-old B6 mice followed by OVA immunization. Similar to the LCMV model, mice having received *Cish*-silenced OT-II $CD4^+$ T cells had reduced serum mtDNA and inflammatory cytokine serum concentrations on day 8 after immunization as well as lower proinflammatory gene transcripts in splenocytes compared to mice with control-silenced cells (Fig. 8h-j). Moreover, mice having received *Cish*-silenced OT-II $CD4^+$ T cells had increased frequencies and absolute numbers of TFH cells in the spleen with better antibody responses as shown by increased serum anti-OVA antibodies (Fig. 8k and Extended Fig.8e).

Discussion

Here, we show that T cell responses from older adults are pro-inflammatory due to excessive release of mtDNA and other amphisomal products, thereby assigning T cells a regulatory role in inflammaging that goes beyond cytokine production. At a center stage in this age-associated response pattern is a lysosomal defect due to the accelerated proteasomal degradation of ATP6V1A and the associated failure in lysosomal acidification. Tagging of ATP6V1A for degradation is facilitated by the scaffolding activity of CISH, the transcription of which is induced by T-cell receptor (TCR) activation in older T cells that have reduced activity of the transcriptional repressor TCF1. We have previously reported that replenishment of lysosomes is impaired in activated T cells undergoing proliferation due to a reduced expression of the transcription factor TFEB that controls the transcription of lysosomal genes[26]. The defect in lysosomal acidification is an independent additional

mechanism in T cell responses from older adults identifying several age-associated changes converging on lysosomal dysfunction. Taken together, T cells from older adults litter their immediate environment with mitochondrial and other cellular products that have been targeted for lysosomal degradation, a defect that can be prevented by silencing *CISH*.

Lysosomal degradation of damaged mitochondria is initiated by the formation of double-membraned autophagosome that seal the whole mitochondrion, or its damaged area followed by fusion with lysosomes to form autolysosomes and ultimately the degradation of mitochondria in the autolysosomal lumen[38, 39]. In some types of cells, before fusion with lysosomes, autophagosomes fuse with late endosomes to form the intermediate/hybrid organelle amphisomes, which contain both late endosomal and autophagic cargos[40]. The formation of amphisomes allows autophagosomes to acquire the transport motility from the late endosomes/MVBs, which facilitates their fusion with lysosomes[40]. In several age-related neurodegenerative diseases, a defect of lysosomal clearance results in the abnormal intracellular accumulation of amphisomes, leading to amphisome/plasma membrane fusion and subsequent amphisome-mediated extracellular secretion of luminal contents[40, 41]. Likewise, we find an intracellular accumulation of amphisomes in activated naïve $CD4^+$ T cells from older adults. Due to lysosome dysfunction in these T cells, amphisomes are no longer targeted for degradation but fuse with the plasma membrane and release their luminal contents including damaged mitochondria to the extracellular milieu. Released damaged mitochondria provide a source of circulating mtDNA, which is one of the most important inducers of inflammaging[42, 43]. mtDNA activates innate recognition receptors, including cGAS-STING and Toll-like receptors, resulting in inflammasome activation and production of type I interferon and proinflammatory cytokines[44, 45]. Previous studies on inflammaging have mostly focused on the cytosolic leakage of mtDNA in innate immune cells upon activation and cellular stress [45]. Here, we find that secretion of mtDNA is inherent in a normal $CD4^+$ T cell response and heightened with T cells of older adults.

The autophagy-lysosome pathway is essential to maintain organelle homeostasis and thus to prevent age-associated inflammation[46, 47]. Previous studies have shown an age-associated decline of macroautophagy in resting human T cells[48, 49]. The underlying mechanisms for this defect are poorly understood. Transcriptomic analyses so far have failed to identify autophagy-related gene signatures associated with age in T cells[50]. One possible mechanism is an increase in MAPK p38 activity in selected older T cells that inhibits ATG9 activity[51]. Previous studies were mostly done on basal autophagy in resting cells that is different from activation-induced autophagy[52]. Our studies were done on activated T cells that in contrast to resting T cells are anabolic undergoing organelle and mitochondrial biogenesis. Here, the upstream mechanism of increased MVB and amphisome accumulation was a defective clearance function of lysosomes.

Deficiency in TCF1 expression is one hallmark of T cell aging. One of the target genes of TCF1 is *CISH*, a member of the SOCS family (Fig. 1h). TCF1 has been shown to bind to the *CISH* promoter repressing its transcription[53]. CISH acts as a scaffolding protein by binding ATP6V1A and facilitating its ubiquitination and proteasomal degradation. ATP6V1A is an essential component of the proton pump V-ATPase that maintains lysosomal acidification. Excessive induction of *CISH* transcription in activated naïve $CD4^+$ T cells

from older individuals increased ATP6V1A degradation and impaired lysosomal clearance of autophagosomes, thereby leading to intracellular accumulation of damaged mitochondria and amphisomes resulting in exocytosis of damaged mitochondria. In addition to defective clearance, age-related mitochondrial defects may contribute to their accumulation and aggravate the inflammatory response[3, 25, 54].

In addition to the in vitro data with human cells, we have confirmed a role of CISH in regulating inflammation in murine models of antigen-driven T cell responses. Increasing the number of antigen-specific T cells by adoptively transferring TCR-transgenic T cells induced an increase in the serum concentrations of mtDNA in the LCMV infection as well as the ovalbumin immunization model. Mice adoptively transferred with antigen-specific *Cish*-silenced $CD4^+$ T cells had reduced serum mtDNA and proinflammatory cytokine concentrations, confirming that mtDNA was derived from the responding T cell population and CISH dependent.

Further studies are needed to assess whether in addition to aging, increased CISH expression accounts for increased inflammation via mtDNA release in several settings of chronic T cell activation. CISH has been reported to be highly induced in the chronic LCMV infection model[53]. CISH is also highly expressed in tumor-infiltrating lymphocytes[55]. In both models, CISH has been implicated to account for attenuated TCR signaling in exhausted T cells, but it may also contribute to the chronic inflammatory response in these conditions. Of particular interest, increased serum mtDNA derived from T cells may contribute to the inflammatory cytokine release syndrome (CRS) commonly observed in patients receiving adoptive CAR-T cell therapy[56, 57, 58]. *CISH* knockout in adoptively transferred T cells is currently explored in a human clinical trial for the treatment of gastrointestinal cancer patients (https://clinicaltrials.gov/ct2/show/NCT04426669)[59]. Although the trial was originally conceived to combat exhaustion, our data suggest that it may also show a reduced incidence and severity of CRS.

mtDNA release at the height of the T cell response will hyperstimulate innate immunity, which may be beneficial to control a viral infection, but also cause tissue damage. In addition, this pro-inflammatory environment will also impact the adaptive immune response and T cell differentiation. A previous study found that impaired lysosomal function directs T cell differentiation toward an inflammatory lineage, exacerbating an inflammatory response[60]. In contrast to this positive feedback loop, excessive inflammation may also curtail the generation of adaptive immune response[17, 20, 61]. Upregulation of PD-L1 on inflammatory macrophages inhibits T cells from older adults that express more PD-1 after activation[26, 62]. Excess type I interferon reduces the number of antigen-specific IFN-γ^+ $CD4^+$ T cells. Blockade of type I interferon signaling resulted in increased numbers of IFN-γ^+ $CD4^+$ T cells and thus enhanced virus clearance[63, 64]. In support of such an immunosuppressive effect, we found mice having received *Cish*-silenced SMARTA $CD4^+$ T cells had less inflammatory responses after acute LCMV infection compared to mice having received control-silenced cells. A similar improved adaptive immune response was seen in an immunization model, where TFH cell frequencies and serum anti-OVA antibodies were increased after transfer of *Cish*-silenced OT-II $CD4^+$ T cells.

In summary, we describe that lysosomal function in responding T cells is essential to maintain a healthy immune microenvironment with low inflammation and superior outcome in antibody responses. Impaired lysosomal activities in T cell responses from older individuals promotes amphisomal exocytosis of intracellular waste including damaged mitochondria and mtDNA that induces local activation of inflammatory cells. It should be noted that the inflammation described here occurs in an acute immune response of largely healthy, older individuals, such as in an acute infection or a vaccination. Whether the same mechanisms contribute to the chronic subtle system inflammation seen in older adults is possible but remains to be seen. Inflammaging is more prevalent in frail individuals, and one of the limitations of our study is that we did not study the relationship to frailty. Irrespective of how systemic the process is that we are describing, with the excessive induction of *CISH* transcription we have identified a key mechanism that can be targeted to reduce T cell-dependent inflammation and improve adaptive immunity in older individuals.

Methods

Study population and cell isolation

PBMCs were obtained from leukocyte reduction chambers of 57 young (20 to 35 years old) and 64 older (65 to 85 years old) healthy blood donors of both genders, purchased from the Stanford Blood Center (Palo Alto, CA, USA) and the Mayo Clinic Blood Center (Rochester, MN, USA). The study was in accordance with the Declaration of Helsinki, approved by the Stanford Institutional Review Board and the Mayo Clinic Institutional Review Board. Samples had been deidentified except for age range and gender. Human naïve $CD4^+$ T cells were purified using a $CD4^+$ T cell enrichment cocktail kit (15062, STEMCELL Technologies), followed by negative selection with anti-CD45RO magnetic beads (19555, STEMCELL Technologies). Human naïve $CD8^+$ T cells and naïve B cells were purified by using human naïve $CD8^+$ T Cell Isolation Kit (19258, STEMCELL Technologies) and Human Naïve B Cell Isolation Kit (17254, STEMCELL Technologies), respectively. Human $CD14^+$ monocytes were isolated by positive selection with CD14 MicroBeads (130050201, Miltenyi Biotec).

Cell culture

Freshly isolated human naïve $CD4^+$ T cells or naïve $CD8^+$ T cells were activated at a density of 5 x 10^5/ml with anti-CD3/anti-CD28 Dynabeads (11132D, Thermo Fisher Scientific) in RPMI 1640 (Sigma-Aldrich) supplemented with 10% fetal bovine serum (FBS) and penicillin and streptomycin (100 U/ml, Thermo Fisher Scientific). Freshly isolated human naïve B cells were expanded by using CellXVivo Human B Cell Expansion Kit (CDK005, R&D system) for 5 days. Freshly isolated human $CD14^+$ monocytes were stimulated with 20 ng/ml M-CSF for 4 days followed by 100 ng/ml LPS for 1 day. Freshly isolated mouse naïve $CD4^+$ T cells (19765, STEMCELL Technologies) were activated at a density of 2 x 10^6/ml in plates coated with anti-CD3 (8 μg/ml; 16-0032-82, eBioscience) and anti-CD28 Ab (8 μg/ml; 16-0281-82, eBioscience) in culture medium supplemented with interleukin-2 (IL-2) (10 ng/ml; 21212, PeproTech).

Transfection

Freshly isolated human naïve $CD4^+$ T cells or naïve $CD8^+$ T cells were transfected with either SMARTpool negative control small interfering RNA (siRNA), SMARTpool *TCF7* siRNA, SMARTpool *CISH* siRNA, SMARTpool *ATP6V1A* siRNA (all from Dharmacon), or pCMV6-Entry Mammalian or Human *CISH* expression vector (NM_145071, both from Origene) using the Amaxa Nucleofector system and the P3 primary cell Nucleofector Kit (Lonza). After transfection, cells were rested for 2 hours before being activated by anti-CD3/anti-CD28 Dynabeads for 3 or 5 days. For lentiviral transduction, naïve $CD4^+$ T cells were transduced with a lentiviral vector expressing either scrambled control, *TCF7*, RFP-LC3 or RFP-GFP-LC3 (as the autophagic flux probe). After overnight culture, cells were activated by anti-CD3/anti-CD28 Dynabeads for 3 days.

Immunoblotting

Cells were washed with cold PBS and lysed in commercial RIPA buffer supplemented with phenylmethylsulfonyl fluoride and protease and phosphatase inhibitors (sc-24948, Santa Cruz Biotechnology) for 30 min on ice. Proteins were separated on denaturing 4-15% (15-well) SDS–polyacrylamide gel electrophoresis (4561086, Bio-Rad), transferred onto nitrocellulose or PVDF membrane (1704270, Bio-Rad), and probed with antibodies to TCF1 (C46C7, #2206, 1:1000), β-actin (D6A8, #8457), 1:1000, CISH (D4D9, #8731, 1:1000), LC3B (D11, #3868, 1:1000), COXIV (3E11, #4850, 1:1000, all Cell Signaling Technology), and ATP6V1A (ab199326, Abcam, 1:1000). Blotting membranes were developed by incubation with horseradish peroxidase (HRP)–conjugated secondary antibodies (Cell Signaling Technology, #7074, 1:2500) followed by treating with the Chemiluminescent Western blot Detection Substrate (Thermo Fisher Scientific).

Flow cytometry

For cell surface staining, cells were incubated with fluorescently conjugated antibodies in phosphate-buffered saline (PBS) supplemented with 2% FBS at 4°C or on ice for 30 min. For intracellular protein staining, cells were treated with FOXP3 Fix/Perm Buffer Set (421403, BioLegend) followed by incubation with fluorescently conjugated antibodies at room temperature for 60 min. Dead cells were excluded from the analysis using LIVE/DEAD Fixable Violet Dead Cell Stain Kit (ThermoFisher). Staining for flow cytometry was done with antibodies to AF-700 CD4 (anti-human: RPA-T4, #557922; anti-mouse: RM4-5, #557956, 1:100), FITC CD8 (anti-human: RPA-T8, #561948; anti-mouse: 53-6.7, #553031; 1:100) and PE-CXCR5 (anti-mouse: 2G8, #561988, 1:50) all BD Biosciences), TCF1 (anti-human: 7F11A10, #655208, 1:100), AF647 PD-1 (anti-mouse: 29F.1A12, #135230, 1:100), BV421 CD44 (anti-mouse: IM7, #103040, 1:100), PE-Cy7 CD62L (anti-mouse: MEL-14, #104418, 1:100), APC-Cy7 CD69 (anti-mouse: H1.2F3, #104525, 1:100) and AF647 SLAM (anti-mouse: TC15-12F12.2; 1:50, #115918, all Biolegend). Mouse CXCR5 was stained with biotin-conjugated anti-CXCR5 (2G8, 1:50, BD Biosciences) followed by staining with allophycocyanin-streptavidin (BD Biosciences). Intracellular CISH was stained with primary anti-CISH (D4D9, #8731, 1:100, Cell Signaling Technology) followed by staining with BV421 anti-rabbit IgG (#406410, 1:200, Biolegend). Cells were analyzed on an LSR Fortessa (BD Biosciences). Flow cytometry data were analyzed using FlowJo.

RNA isolation and quantitative RT-PCR

Total RNA was isolated by using RNeasy Plus Mini Kit (74134, QIAGEN) and was reverse transcribed using SuperScript VILO cDNA Synthesis Kit (11754, Invitrogen). Quantitative polymerase chain reaction (qPCR) was performed on the ABI 7900HT system (Applied Biosystems) using Power SYBR Green PCR Master Mix (4368706, Thermo Fisher Scientific) according to the manufacturer's instructions. Oligonucleotide primer sets used in this study are shown in table 1.

Proteasome activity assay

Naïve $CD4^+$ T cells were activated for 3 days and homogenized with Pierce IP Lysis Buffer (#87787, ThermosFisher). Proteasomal degradation was quantified by using Proteasome Activity Assay Kit (ab107921, Abcam) following the manufacturer's manual. Briefly, samples were incubated with or without proteasome inhibitor, proteasome substrate and assay buffer for 30 min at 37°C. Fluorescence was determined on a fluorometric plate reader BioTek Synergy H1 at 350/440 nm.

Lysosomal acidification and proteolytic activity assay

For analyzing lysosomal acidification, day 3-stimulated naïve $CD4^+$ T cells were treated with 1 μM LysoSensor (L7535, Thermo Fisher Scientific) diluted in prewarmed culture medium and incubated for 30 min at 37°C, followed by washes with ice-cold PBS. LysoSensor fluorescence was quantified by flow cytometry. For examining lysosomal proteolytic activities, cells were treated with DQ-BSA (5 μg/ml; D12050, Thermo Fisher Scientific) diluted in prewarmed culture medium and further incubated at 37°C for 6 hours. After incubation, cells were briefly washed once with ice-cold PBS containing 2% FBS. Fluorescence of cleaved DQ-BSA was analyzed by flow cytometry.

Immunoprecipitation of ATP6V1A

Naïve $CD4^+$ T cells were transfected with control or *CISH* siRNA and activated for 3 days, with the last 8 hours in the presence of 1 μM MG132 (CaymanChemical). Cells were lysed using the Lysed Pierce IP Lysis Buffer (ThermoFisher) and incubated with anti-ATP6V1A Ab (ab199326, Abcam 1:1000) at 4°C overnight. ATP6V1A was immunoprecipitated by treating the whole-cell lysates with Protein G Agarose (sc-2002, Santa Cruz Biotechnology) at 4°C for 2 hours. After washing 5 times, immune complexes were boiled for 15 minutes in Laemmli Sample Buffer (#1610747, Bio-Rad). Samples were loaded for electrophoresis and subsequently transferred onto PVDF membranes before immunoblotting for specific markers.

Transmission electron microscopy

In vitro day 3-activated naïve $CD4^+$ T cells or sorted mouse SMARTA $CD4^+$ T cells at day 6 after LCMV infection were fixed overnight in 1% glutaraldehyde and 4% formaldehyde in 0.1 M phosphate buffer, pH 7.2. Cells were then rinsed for 30 minutes and postfixed in phosphate-buffered 1% OsO4 for one hour. After three washes in water, cells were *en bloc* stained with 2% uranyl acetate for 30 minutes. After *en bloc* staining, cells were rinsed, dehydrated, and embedded in Spurr resin. Cells were then polymerized in a 60°C

oven overnight. Sections (60 to 80 nm) were treated with uranyl acetate and lead citrate and viewed on a JEOL 1400 Plus electron microscope. Images were collected of every cell profile within four grid squares of a single thin section of each sample. 15 or 20 cells were imaged for each donor. Damaged mitochondria were defined as either no visible cristae, surrounded by a phagophore or being located inside an amphisome. Image acquisition and analysis were conducted by an examiner blinded to the kind of the sample (e.g., age, silencing condition, etc).

Human and mouse mitochondrial DNA quantification

Absolute human and mouse mtDNA copy numbers were quantified by using the Absolute Human Mitochondrial DNA Copy Number Quantification qPCR Assay Kit (#8948) and the Absolute Mouse Mitochondrial DNA Copy Number Quantification qPCR Assay Kit (#M8948, both ScienCell), respectively. The human or mouse mtDNA primer sets provided in the kit recognize and amplify a conserved region of human or mouse mtDNA. The reference DNA sample with known human or mouse mtDNA copy number served as a reference for calculating the absolute mtDNA copy numbers of target samples.

Mice, adoptive transfers, LCMV infection and OVA immunization

For the SMARTA/LCMV infection model, naïve $CD4^+$ T cells specific to the GP66-77 epitope of LCMV (Armstrong) obtained from 5- to 8-week-old SMARTA TCR transgenic mice (CD45.1, a gift from R. Ahmed at Emory University) were activated in plates coated with anti-CD3/anti-CD28 Ab. To avoid a transient silencing effect in vivo by transfection, retroviral vectors expressing either scrambled control or *Cish* shRNA (5′-CAGTTATACAGTATTTATTTA-3′) were generated using the Plat-E Retroviral Packaging Cell Line (Cell Biolabs, Inc) and T cells were transduced on days 1 and 2 after activation. On day 6 after activation, retrovirus-transduced Amcyan-positive SMARTA cells were sorted. 1×10^5 transduced cells were intravenously transferred to 5- to 8-week-old female C57BL/6 (CD45.2) mice (the Jackson laboratory). One day after transfer, mice were infected intraperitoneally with 2×10^5 plaque-forming units (PFU) of LCMV Armstrong. On day 6 after infection, spleen and blood were harvested and analyzed. For the OT-II/OVA immunization model, naïve $CD4^+$ T cells specific to the chicken ovalbumin 323-339 peptide obtained from 5- to 8-week-old OT-II TCR transgenic mice (CD45.1, the Jackson Laboratory) were activated and retrovirally transduced as described for SMARTA cells. On day 6 after activation, retrovirus-transduced Amcyan-positive OT-II cells were sorted; 1×10^5 transduced cells were intravenously transferred to 5- to 8-week-old female C57BL/6 (CD45.2) mice (the Jackson laboratory). One day after transfer, mice were immunized with 100 μg OVA (Biosearch Technologies) precipitated in 100 μL 5% alum (aluminum potassium sulfate, MilliporeSigma). On day 8 after immunization, spleen and blood were harvested and analyzed. Mice were house at a temperature of 23°C ± 2°C, relative humidity of 30% to 40%, and a 12:12-h light dark cycle. All animal experiments were approved by and performed following the guidelines of the Mayo Clinic Administrative Panel on Laboratory Animal Care Committee.

ELISA for serum cytokines and antibodies

Proinflammatory cytokines (TNF-α, IL-1β and IL-6) serum concentrations were measured using Enzyme-linked immunosorbent assay (ELISA) kits (ThermoFisher). Briefly, ELISA plates coated with cytokine capture antibody were washed, blocked, and incubated with 50 μl of serum samples for 2 hours. In parallel, a standard curve was made by incubating 2-fold serial dilutions of the standards. Plates were then washed and incubated with biotin-conjugated detection antibodies for 1 hour. After washing, plates were incubated with Streptavidin-HRP. Bound antibodies were detected by adding 3,3′,5,5′-tetramethylbenzidine substrate (TMB Solution) followed by plate reading for absorbance at 450 nm. Cytokines levels were calculated based on a standard curve. OVA-specific IgG1 was measured by using the anti-Ovalbumin IgG1 (mouse) ELISA Kit (#500830, CaymanChemical) according to the manufacturer's instructions.

LCMV viral RNA quantification

Total RNA of the spleen or kidney was isolated and reverse-transcribed to cDNA using the SuperScript VILO cDNA Synthesis Kit (#11754050, ThermoFisher). The kit contains random primers that can reverse-transcribe LCMV viral RNA to cDNA. qPCR was performed by using the previously reported LCMV GP specific primers (forward: 5'- CATTCACCTGGACTTTGTCAGACTC-3'; reverse: 5'-GCAACTGCTGTGTTCCCGAAAC-3')[65]. RNA isolated from the spleen from non-infected mice was used as negative control.

Confocal microscopy

Day 3-stimulated naïve $CD4^+$ T Cells were fixed in 4% paraformaldehyde, permeabilized with 0.2% Triton X-100, and incubated with primary antibodies to CD63 (#556019, BD Pharmingen, 1:100) together with antibodies to CISH (ab88383, Abcam 1:100), ATP6V1A (ab199326, Abcam, 1:100), LC3B (D11, #3868, Cell Signaling Technology, 1:100) or COX IV (3E11, #4850, Cell Signaling Technology, 1:100) at 4°C overnight. Incubation with secondary antibodies was performed at room temperature for 2 hours using Alexa Fluor 488–conjugated AffiniPure Donkey anti-Rabbit immunoglobulin G (IgG), Cy3-conjugated AffiniPure Donkey anti-Mouse IgG (Jackson Immuno Research Laboratories), Alexa Fluor 647-conjugated goat anti-rabbit IgG H&L or Alexa Fluor 488-conjugated goat anti-mouse IgG H&L (Abcam), all at 1:500. The images were analyzed using an LSM 980 microscope system with the ZEN 2010 software (Carl Zeiss) and a 63× oil immersion objective (Carl Zeiss).

Statistics and reproducibility:

Statistical analysis was performed using the Prism 8.0 software. Two-tailed paired or unpaired Student's t tests were used for comparing two groups. One-way analysis of variance (ANOVA) with Tukey's post hoc test was used for multigroup comparisons. Sample sizes to identify differences in mtDNA release, CISH or TCF1 expression between young and old adults were chosen to ensure 80% power with a level of significance of 5% for a difference of their means of 1.5 standard deviation ($n \geq 10$). Data distribution was not formally tested but assumed to be normal. To assess the effect of in vitro intervention

(e.g., gene silencing, pharmacological inhibition), we used paired testing with sample sizes of 3 to 5. Sample sizes for the mouse studies were similar to those reported in previous publications. For imaging experiments, we used a sample size of 15-20 sections for each sample with a total of 5 samples in each group. The investigators examining the images were blinded to the nature of the sample. Experiments were not randomized. $P < 0.05$ was considered statistically significant. Statistical details and significance levels can be found in figure legends.

Extended Data

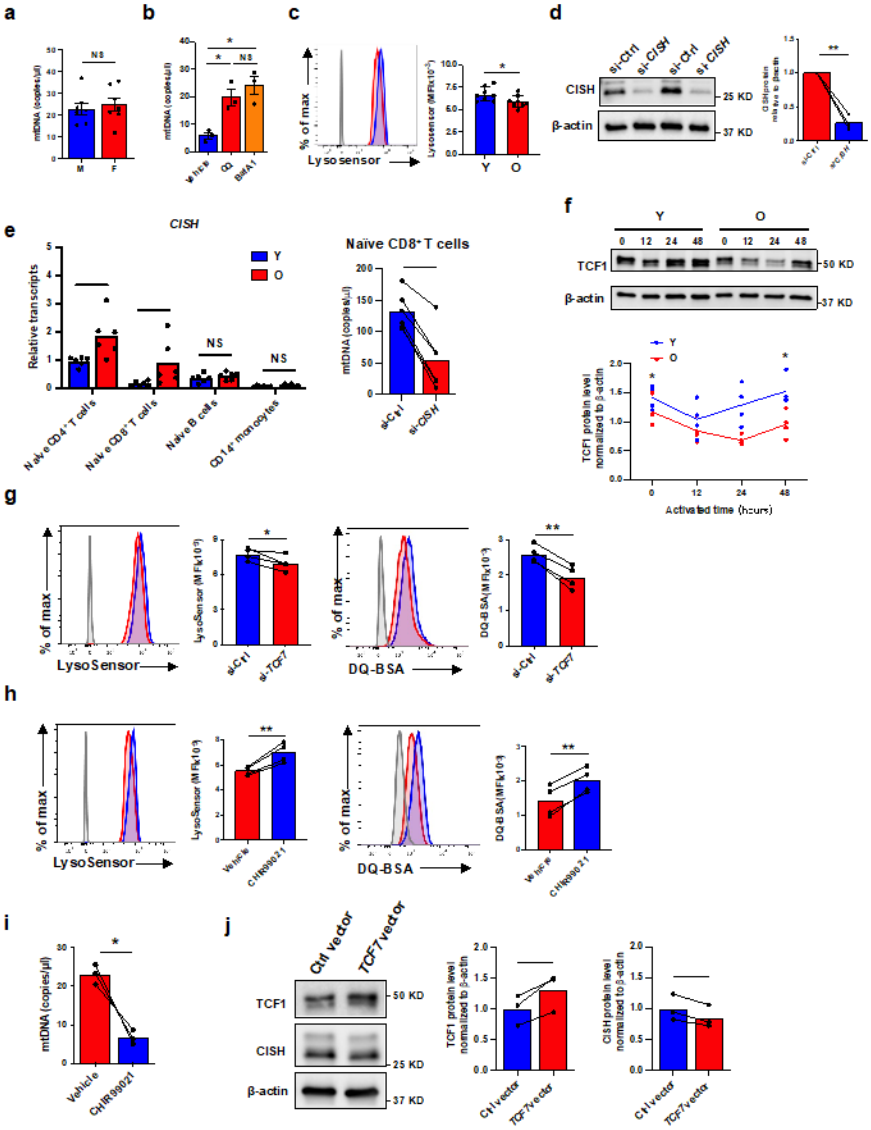

Extended Data Fig. 1. related to Fig. 1: TCF1 prevents mtDNA release by promoting lysosomal activity.

a, b, Naïve CD4$^+$ T cells from older 7 females and 7 males were activated for 3 days **(a)**. Cells from 3 young adults were activated in the presence or absence of 10 μM CQ or 5 nM BafA1 **(b)**. mtDNA levels in the culture supernatants were determined. **c**,

Lysosomal acidification was determined by flow cytometry-based analysis of LysoSensor in day 3-stimulated naïve CD4$^+$ T cells comparing 8 young and 8 older individuals. **d**, Naïve CD4$^+$ T cells from 3 older individuals were transfected with control or *CISH* siRNA and activated for 3 days. Reduced CISH protein expression after silencing was confirmed by immunoblotting. **e**, *CISH* transcripts in naïve CD4$^+$ T cells and naïve CD8$^+$ T cells stimulated for 3 days, in naïve B cells and CD14$^+$ monocytes stimulated for 5 days comparing 6 young and 6 older individuals (left); mtDNA levels in culture supernatants of day 3-activated naïve CD 8$^+$ T cells from 6 older individuals (right). **f**, TCF protein levels in naïve CD4$^+$ T cells at indicated time points after stimulation comparing 4 young and 4 older individuals. **g**, Naïve CD4$^+$ T cells from 4 young individuals were transfected with control or *TCF7* siRNA and activated for 3 days. Lysosomal acidification (left) and proteolytic activities (right) were determined by flow cytometry-based analysis of LysoSensor and DQ-BSA-treated cells, respectively. **h, i**, Naïve CD4$^+$ T cells from older individuals were activated for 3 days in the presence of either vehicle or 100 nM of CHIR99021. Lysosomal acidification, proteolytic activities (n=4) **(h)** and supernatant mtDNA levels (n=3) **(i)** were determined. **j**, TCF1 and CISH protein in day 3-stimulated naïve CD4$^+$ T cells from 3 older individuals after transfection with pCMV6 control vector or *TCF7*-expressing vector. Data are presented as mean ± s.e.m. Comparison by two-tailed unpaired *t* test (a,c,e,f) or two-tailed paired *t* test (b,d,e,g-j). **P* < 0.05, ***P* < 0.01; NS, not significant.

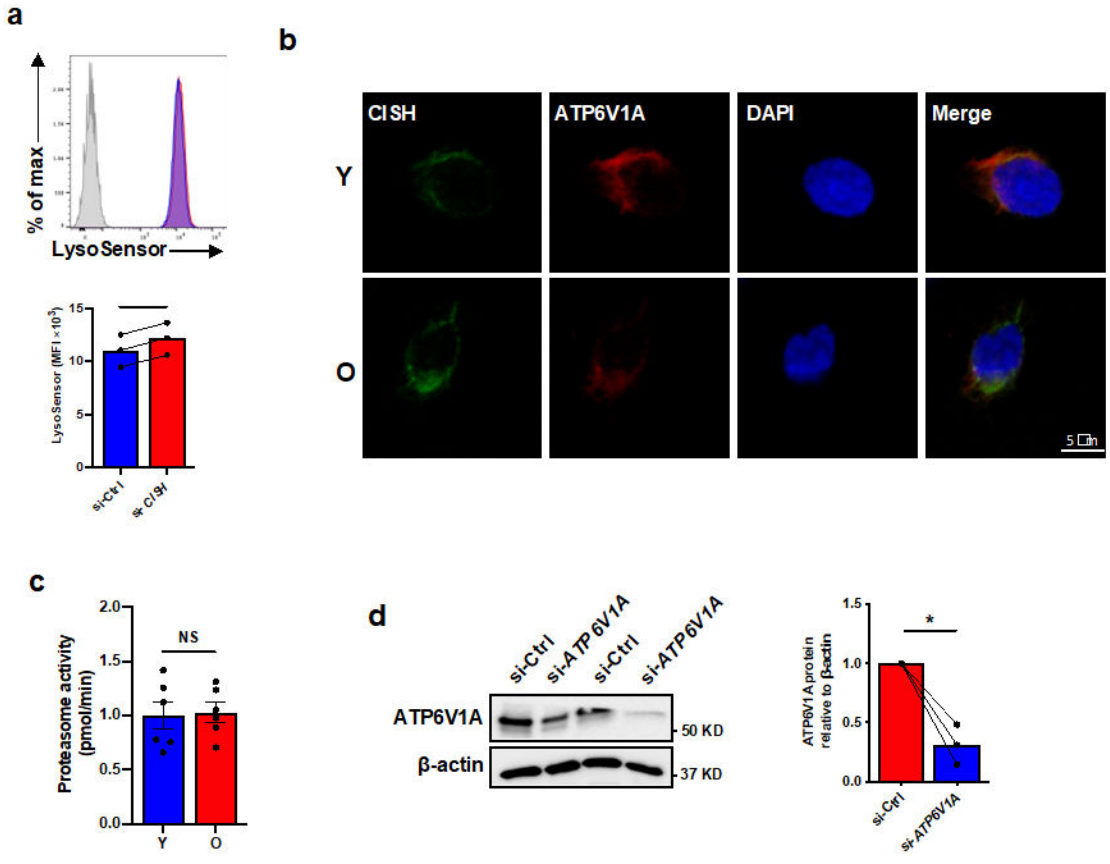

Extended Data Fig. 2. related to Fig. 2: Silencing of *CISH* and *ATP6V1A* expression in day 3-activated naïve CD4$^+$ T cells.

a, Naïve CD4$^+$ T cells were transfected with control or *CISH* siRNA and activated for 3 days (n=3). Lysosomal acidification was determined by flow cytometry-based analysis of LysoSensor-treated cells. **b**, Naïve CD4$^+$ T cells from a young and an older individual were co-stained with anti-CISH (green) and anti-ATP6V1A Ab (red). Confocal images representative of three independent experiments are shown. **c**, Proteasome activity in day 3-activated naïve CD4$^+$ T cells from 6 young and 6 older individuals. **d**, Naïve CD4$^+$ T cells from 3 young individuals were transfected with control or *ATP6V1A* siRNA and activated for 3 days. Reduced *ATP6V1A* protein expression after silencing was confirmed by Western blotting. Data are presented as mean ± s.e.m. Comparison by two-tailed paired *t* test (a,d) or two-tailed unpaired *t* test (c). **P* < 0.05; NS, not significant.

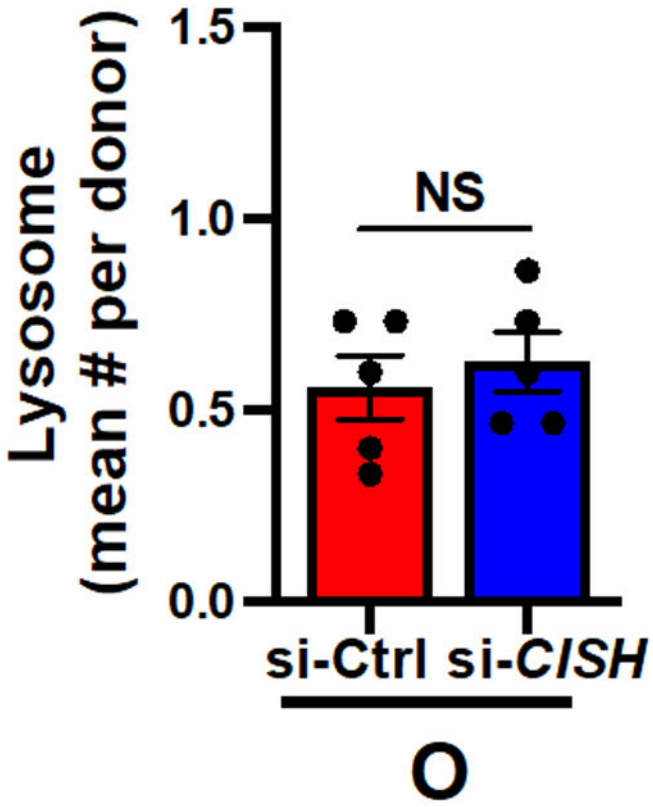

Extended Data Fig. 3. related to Fig. 4: CISH silencing does not affect the number of lysosomes per cell.

Quantitative assessment of lysosome numbers in day 3-activated naïve CD4$^+$ T cells from 5 old individuals after CISH silencing. Image acquisition and analysis were performed by an examiner blinded to the nature of the specimen. 15 sections were analyzed for each donor, and mean number per section for each donor is shown NS, not significant. Data are presented as mean ± s.e.m. Comparison by two-tailed unpaired *t* test.

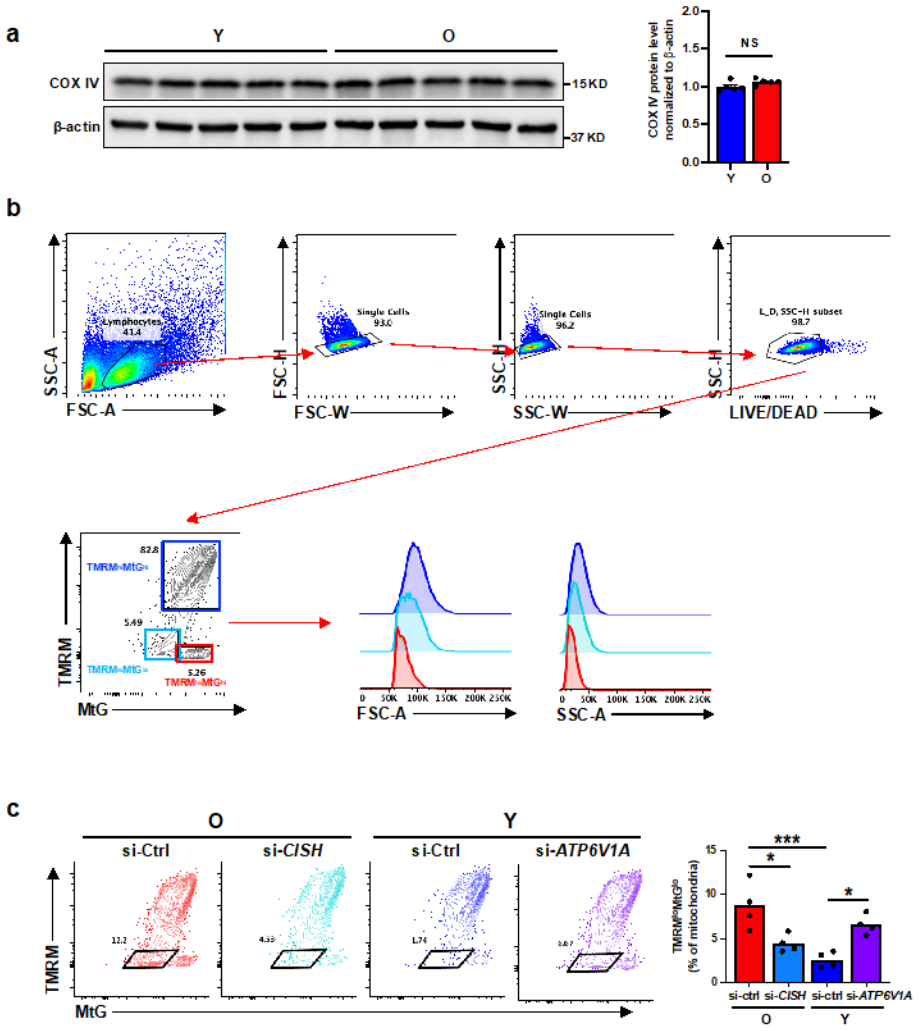

Extended Data Fig. 4. related to Fig. 6: Effect of CISH on mitochondria in activated T cells from older adults.

a, COX IV protein expression in day 3-stimulated naïve $CD4^+$ T cells comparing 5 young and 5 older healthy individuals. **b**, Gating strategy for $TMRM^{hi}MtG^{hi}$, $TMRM^{lo}MtG^{lo}$ and $TMRM^{lo}MtG^{hi}$. $TMRM^{lo}$ cells had reduced cell size (low FSC) and reduced density (low SSC) distinct from apoptotic cells. **c**, Frequencies of the $TMRM^{lo}MtG^{lo}$ population in day 3-activated naïve $CD4^+$ T cells from 4 young and 4 older individuals after indicated gene silencing. Data are presented as mean ± s.e.m. Comparison by two-tailed unpaired *t* test (a), one-way ANOVA followed by Tukey's multiple comparison test (c). $*P < 0.05$, $**P < 0.01$ and $***P < 0.001$; NS, not significant.

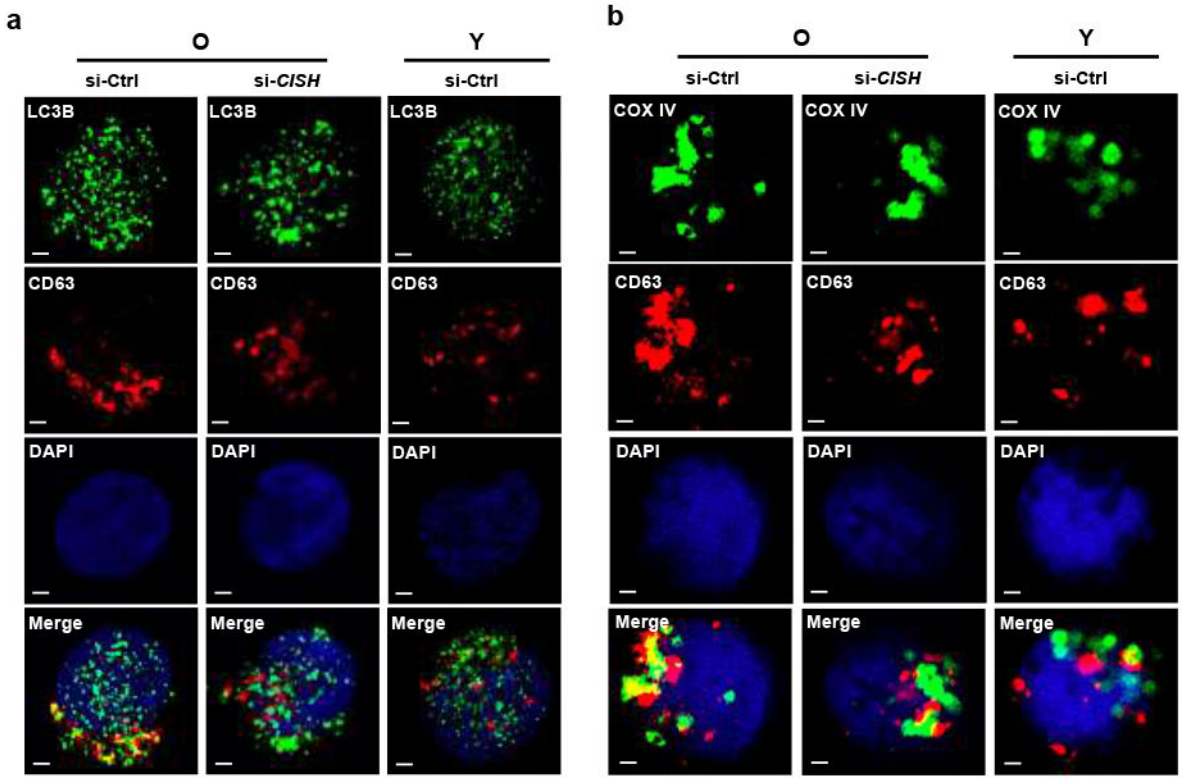

Extended Data Fig. 5. related to Fig. 7: Confocal image analysis of the effect of CISH on mitochondria and MVBs.

a, **b**, Naïve $CD4^+$ T cells from a young and an older individual were transfected with indicated siRNA and activated for 3 days. Cells were costained with anti-CD63 (as MVB marker) and with anti-LC3B (as autophagosome marker) **(a)** or anti-COX IV (as mitochondria marker) **(b)**. Confocal images representative of two independent experiments are shown. Scale bars, 1 μm.

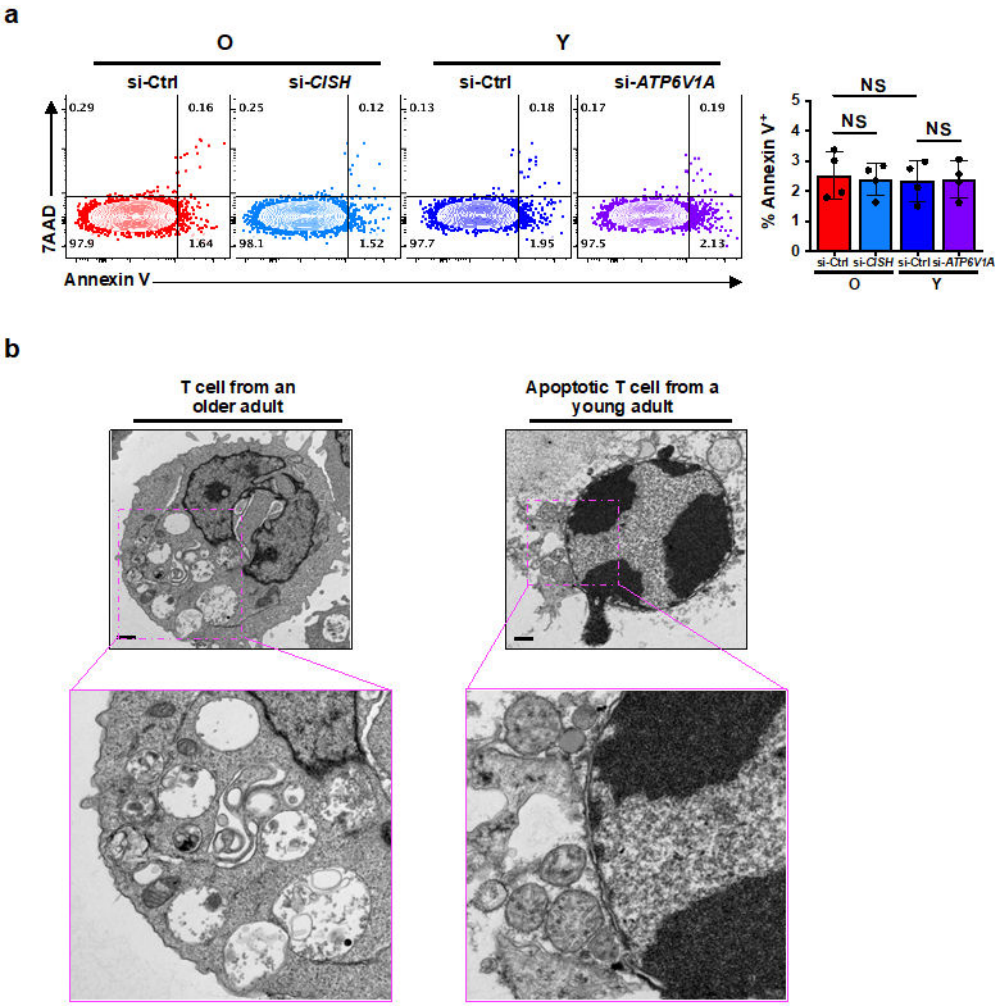

Extended Data Fig. 6. related to Fig. 7: CISH-dependent amphisome-rich T cells from older individuals do not show evidence of apoptosis.

a, Naïve $CD4^+$ T cells were transfected with control or indicated siRNA and activated for 3 days (n=4). Cell apoptosis was examined by staining with Annexin V and 7-AAD. Statistical significance by two-tailed unpaired *t* test. NS, not significant. **b**, Day3-stimulated naïve $CD4^+$ T cells were left untreated or treated with 1 μM Staurosporine for 24 hours. Scale bar, 1 μm. Cells were then processed for TEM. Data are presented as mean ± s.e.m.

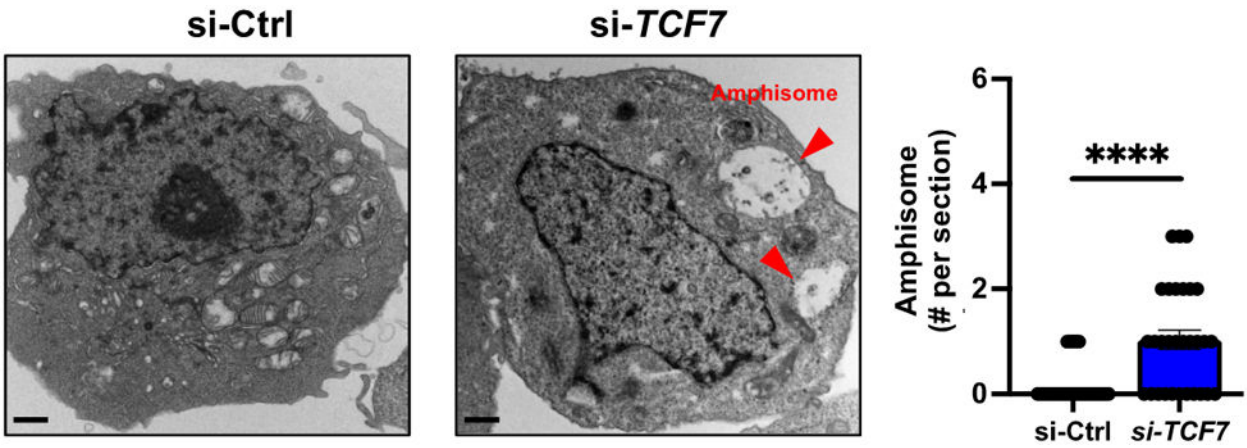

Extended Data Fig. 7. related to Fig. 7: *TCF7* silencing promotes intracellular accumulation of amphisomes.

Naïve $CD4^+$ T cells from young adults were transfected with control or *TCF7* siRNA and activated for 3 days. Cells were then harvested and processed for TEM. Representative 30 TEM images (left) and quantitative plots of amphisome numbers in day 3-activated naïve $CD4^+$ T cells from two young individuals after indicated transfection. Data collection and analysis were conducted in a blinded manner. 15 cells were analyzed for each donor. Scale bar, 1 μm. Data are presented as mean ± s.e.m. Statistical significance by two-tailed unpaired *t* test. **** $P < 0.0001$.

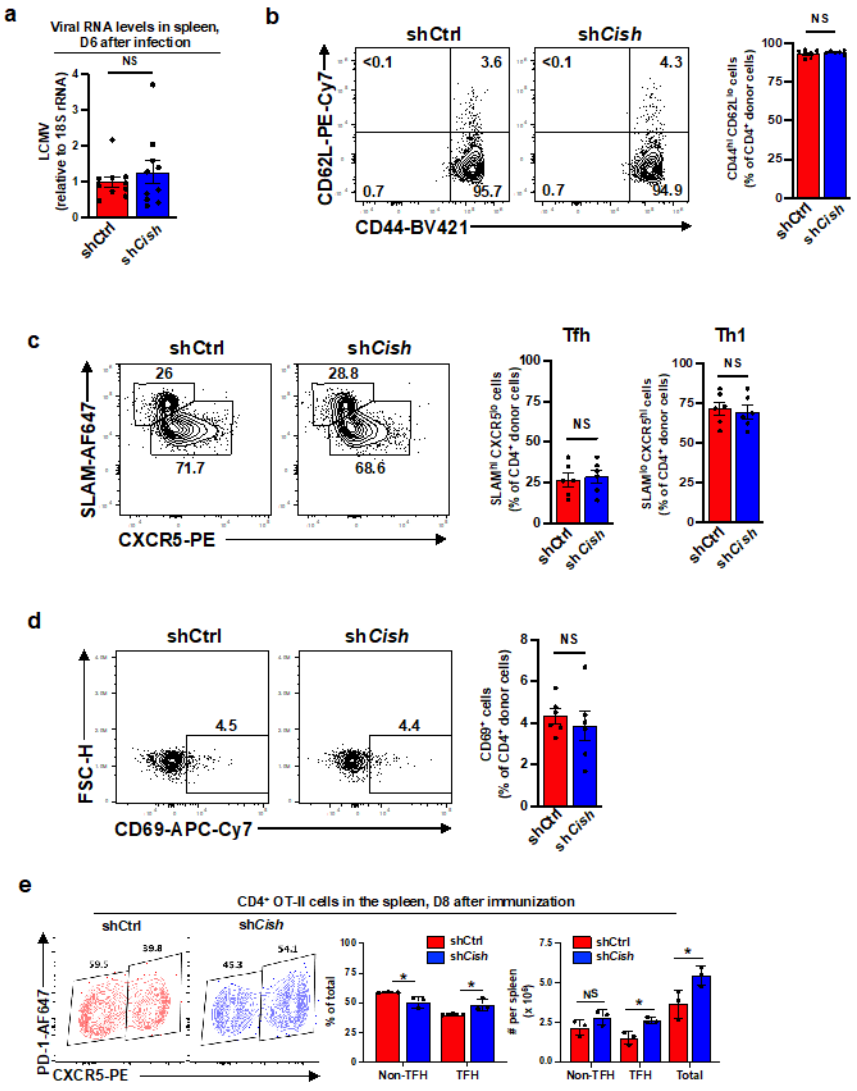

Extended Data Fig. 8. related to Fig. 8: Effect of CISH on T cell responses in vivo.

a-d, SMARTA cells were transduced and adoptively transferred followed by LCMV infection as described in Figure 8. Viral RNA levels in the spleen were determined on day 6, n=10 **(a)**. Frequencies of SMARTA cells with indicated phenotypes in $CD4^+$ donor cells **(b-d)** on day 6 after LCMV infection (n=6). **e**, Mice were reconstituted with sh*Cish* or shCtrl retrovirally transduced naïve OT-II $CD4^+$ T cells (n=3). Frequencies and absolute numbers of TFH and non-TFH OT-II cells in the spleen on day 8 after OVA immunization. Data are presented as mean ± s.e.m. Comparison by two-tailed unpaired *t* test (a-e). $*P < 0.05$; NS, not significant.

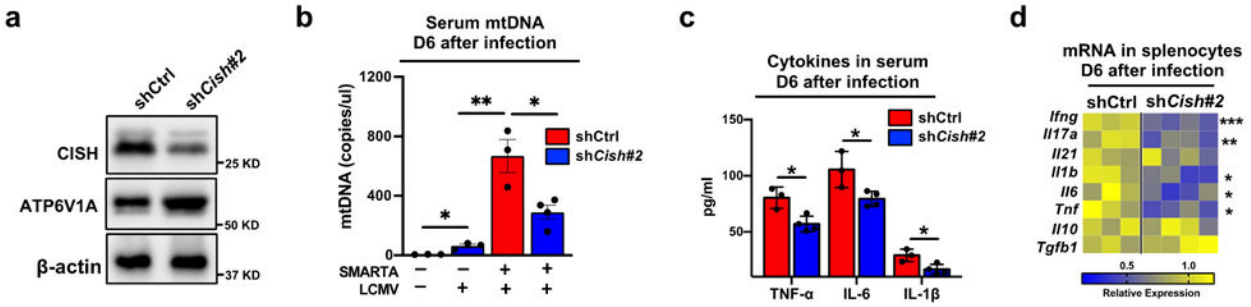

Extended Data Fig. 9. related to Fig. 8: Confirmatory studies with a distinct shRNA to silence *Cish*.

a-d, 1 x 10^5 *Cish* shRNA#2 (5′-AAAACAAGTGTTAGAACACAA-3′) or control shRNA retrovirally transduced Amcyan$^+$ naïve SMARTA CD4$^+$ T cells were adoptively transferred into CD45.2$^+$ naïve recipients followed by LCMV infection. **a**, CISH and ATP6V1A protein expression in transduced cells before adoptive transfer. **b**, Serum mtDNA copies at day 6 after LCMV infection. **c**, Serum proinflammatory cytokines levels on day 6 after LCMV infection. **d**, Gene expression of key inflammatory markers in splenocytes on day 6 after infection. Data are from one experiment with 3-4 mice per group. Data are presented as mean ± s.e.m. Statistical significance by one-way ANOVA followed by Tukey's multiple comparison test (b,d) or two-tailed unpaired *t* test (c). **P* < 0.05, ***P* < 0.01, ****P* < 0.001, and *****P* < 0.0001; NS, not significant.

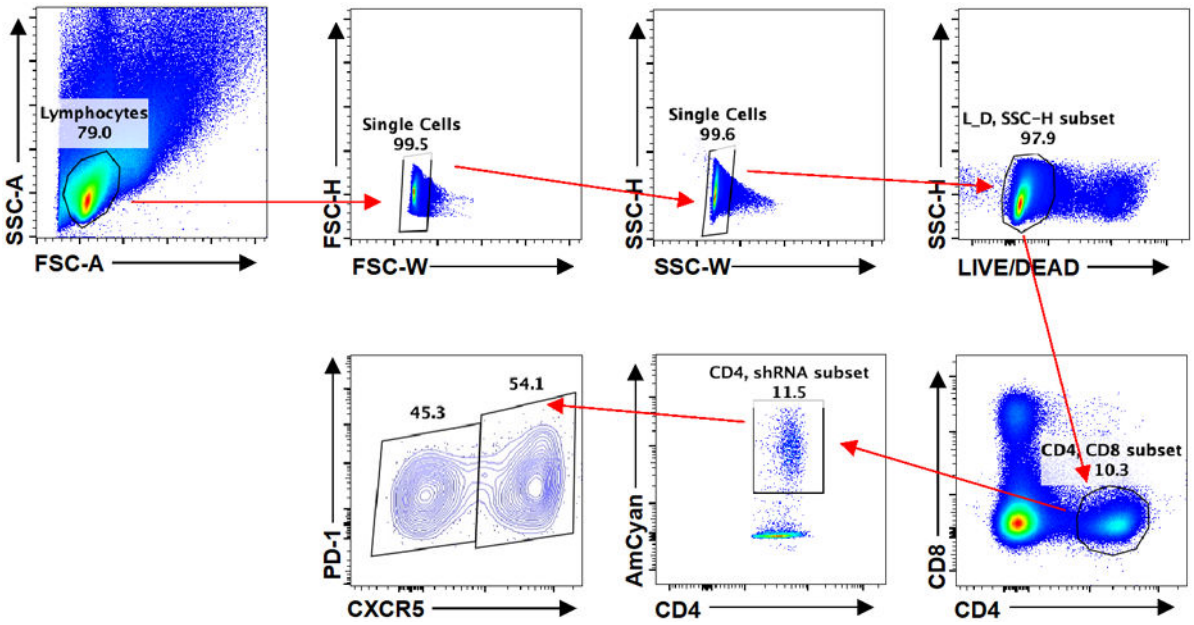

Extended Data Fig. 10. related to Fig. 8: Gating strategy for TFH and non-TFH Amcyan$^+$, successfully transduced cells in the spleen.

Acknowledgments:

We thank the Mayo Clinic Microscopy and Cell Analysis Core for assistance with flow cytometry (Colleen A Moe), cell sorting (Yong Hwan Han) and transmission electron microscopy (Scott Gamb); R. Ahmed (Emory University) for providing SMARTA mice and LCMV-Armstrong.

Funding:

This work was supported by NIH R01 AR042527, R01 HL117913, R01 AI108906, and R01 HL142068 to C.M.W.; R01 AI108891, R01 AG045779, U19 AI057266, and R01 AI129191 to J.J.G. I.S. was supported by T32AG049672 and is a Glenn Foundation for Medical Research Postdoctoral Fellow. The funders had no role in study design, data collection and analysis, decision to publish or preparation of the manuscript. The content is solely the responsibility of the authors and does not necessarily represent the official views of the NIH.

Data availability:

Source data are included with this article. Additional primary experimental data of this study are available from the corresponding author upon request. Sequencing data were obtained from SRA with the accession numbers PRJNA546023 and PRJNA757466.

References

1. Goronzy JJ & Weyand CM Mechanisms underlying T cell ageing. Nat Rev Immunol 19, 573–583 (2019). [PubMed: 31186548]
2. Nikolich-Zugich J. The twilight of immunity: emerging concepts in aging of the immune system. Nat Immunol 19, 10–19 (2018). [PubMed: 29242543]
3. Mittelbrunn M & Kroemer G Hallmarks of T cell aging. Nat Immunol 22, 687–698 (2021). [PubMed: 33986548]
4. Franceschi C, Garagnani P, Parini P, Giuliani C & Santoro A Inflammaging: a new immune-metabolic viewpoint for age-related diseases. Nat Rev Endocrinol 14, 576–590 (2018). [PubMed: 30046148]
5. Ferrucci L & Fabbri E Inflammageing: chronic inflammation in ageing, cardiovascular disease, and frailty. Nat Rev Cardiol 15, 505–522 (2018). [PubMed: 30065258]
6. Goronzy JJ & Weyand CM Successful and Maladaptive T Cell Aging. Immunity 46, 364–378 (2017). [PubMed: 28329703]
7. Pereira BI et al. Sestrins induce natural killer function in senescent-like CD8(+) T cells. Nat Immunol 21, 684–694 (2020). [PubMed: 32231301]
8. Warrington KJ, Takemura S, Goronzy JJ & Weyand CM CD4+,CD28− T cells in rheumatoid arthritis patients combine features of the innate and adaptive immune systems. Arthritis Rheum 44, 13–20 (2001). [PubMed: 11212151]
9. Henson SM, Riddell NE & Akbar AN Properties of end-stage human T cells defined by CD45RA re-expression. Curr Opin Immunol 24, 476–481 (2012). [PubMed: 22554789]
10. Kim C. et al. Activation of miR-21-Regulated Pathways in Immune Aging Selects against Signatures Characteristic of Memory T Cells. Cell Rep 25, 2148–2162 e2145 (2018). [PubMed: 30463012]
11. Zhang H. et al. Aging-associated HELIOS deficiency in naive CD4(+) T cells alters chromatin remodeling and promotes effector cell responses. Nat Immunol 24, 96–109 (2023). [PubMed: 36510022]
12. Kim C. et al. Histone deficiency and accelerated replication stress in T cell aging. J Clin Invest 131 (2021).
13. Li Y. et al. Deficient Activity of the Nuclease MRE11A Induces T Cell Aging and Promotes Arthritogenic Effector Functions in Patients with Rheumatoid Arthritis. Immunity 45, 903–916 (2016). [PubMed: 27742546]
14. Qi Q. et al. Defective T Memory Cell Differentiation after Varicella Zoster Vaccination in Older Individuals. PLoS Pathog 12, e1005892 (2016). [PubMed: 27764254]
15. Lanna A, Henson SM, Escors D & Akbar AN The kinase p38 activated by the metabolic regulator AMPK and scaffold TAB1 drives the senescence of human T cells. Nat Immunol 15, 965–972 (2014). [PubMed: 25151490]

16. Mogilenko DA et al. Comprehensive Profiling of an Aging Immune System Reveals Clonal GZMK(+) CD8(+) T Cells as Conserved Hallmark of Inflammaging. Immunity 54, 99–115 e112 (2021). [PubMed: 33271118]
17. Parmigiani A. et al. Impaired antibody response to influenza vaccine in HIV-infected and uninfected aging women is associated with immune activation and inflammation. PLoS One 8, e79816 (2013). [PubMed: 24236161]
18. Muyanja E. et al. Immune activation alters cellular and humoral responses to yellow fever 17D vaccine. J Clin Invest 124, 3147–3158 (2014). [PubMed: 24911151]
19. Berry MP et al. An interferon-inducible neutrophil-driven blood transcriptional signature in human tuberculosis. Nature 466, 973–977 (2010). [PubMed: 20725040]
20. Fourati S. et al. Pre-vaccination inflammation and B-cell signalling predict age-related hyporesponse to hepatitis B vaccination. Nat Commun 7, 10369 (2016). [PubMed: 26742691]
21. Vukmanovic-Stejic M. et al. Enhancement of cutaneous immunity during aging by blocking p38 mitogen-activated protein (MAP) kinase-induced inflammation. J Allergy Clin Immunol 142, 844–856 (2018). [PubMed: 29155150]
22. Merad M & Martin JC Pathological inflammation in patients with COVID-19: a key role for monocytes and macrophages. Nat Rev Immunol 20, 355–362 (2020). [PubMed: 32376901]
23. Akbar AN & Gilroy DW Aging immunity may exacerbate COVID-19. Science 369, 256–257 (2020). [PubMed: 32675364]
24. Doitsh G. et al. Cell death by pyroptosis drives CD4 T-cell depletion in HIV-1 infection. Nature 505, 509–514 (2014). [PubMed: 24356306]
25. Li Y. et al. The DNA Repair Nuclease MRE11A Functions as a Mitochondrial Protector and Prevents T Cell Pyroptosis and Tissue Inflammation. Cell Metab 30, 477–492 e476 (2019). [PubMed: 31327667]
26. Jin J. et al. FOXO1 deficiency impairs proteostasis in aged T cells. Sci Adv 6, eaba1808 (2020). [PubMed: 32494657]
27. Fang F. et al. Expression of CD39 on Activated T Cells Impairs their Survival in Older Individuals. Cell Rep 14, 1218–1231 (2016). [PubMed: 26832412]
28. Matsui H. et al. Cytosolic dsDNA of mitochondrial origin induces cytotoxicity and neurodegeneration in cellular and zebrafish models of Parkinson's disease. Nat Commun 12, 3101 (2021). [PubMed: 34035300]
29. Queval CJ et al. Mycobacterium tuberculosis Controls Phagosomal Acidification by Targeting CISH-Mediated Signaling. Cell Rep 20, 3188–3198 (2017). [PubMed: 28954234]
30. Jadhav RR et al. Epigenetic signature of PD-1+ TCF1+ CD8 T cells that act as resource cells during chronic viral infection and respond to PD-1 blockade. Proc Natl Acad Sci U S A 116, 14113–14118 (2019). [PubMed: 31227606]
31. Piessevaux J, De Ceuninck L, Catteeuw D, Peelman F & Tavernier J Elongin B/C recruitment regulates substrate binding by CIS. J Biol Chem 283, 21334–21346 (2008). [PubMed: 18508766]
32. Yoshimura A, Naka T & Kubo M SOCS proteins, cytokine signalling and immune regulation. Nat Rev Immunol 7, 454–465 (2007). [PubMed: 17525754]
33. Yim WW & Mizushima N Lysosome biology in autophagy. Cell Discov 6, 6 (2020). [PubMed: 32047650]
34. He MX, McLeod IX, Jia W & He YW Macroautophagy in T lymphocyte development and function. Front Immunol 3, 22 (2012). [PubMed: 22566906]
35. Bektas A. et al. Age-associated changes in human CD4(+) T cells point to mitochondrial dysfunction consequent to impaired autophagy. Aging (Albany NY) 11, 9234–9263 (2019). [PubMed: 31707363]
36. Huotari J & Helenius A Endosome maturation. EMBO J 30, 3481–3500 (2011). [PubMed: 21878991]
37. Yu YR et al. Disturbed mitochondrial dynamics in CD8(+) TILs reinforce T cell exhaustion. Nat Immunol 21, 1540–1551 (2020). [PubMed: 33020660]
38. Palikaras K, Lionaki E & Tavernarakis N Mechanisms of mitophagy in cellular homeostasis, physiology and pathology. Nat Cell Biol 20, 1013–1022 (2018). [PubMed: 30154567]

39. Ma K. et al. Mitophagy, Mitochondrial Homeostasis, and Cell Fate. Front Cell Dev Biol 8, 467 (2020). [PubMed: 32671064]
40. Ganesan D & Cai Q Understanding amphisomes. Biochem J 478, 1959–1976 (2021). [PubMed: 34047789]
41. Eitan E, Suire C, Zhang S & Mattson MP Impact of lysosome status on extracellular vesicle content and release. Ageing Res Rev 32, 65–74 (2016). [PubMed: 27238186]
42. Franceschi C, Garagnani P, Vitale G, Capri M & Salvioli S Inflammaging and 'Garb-aging'. Trends Endocrinol Metab 28, 199–212 (2017). [PubMed: 27789101]
43. Pinti M. et al. Circulating mitochondrial DNA increases with age and is a familiar trait: Implications for "inflamm-aging". Eur J Immunol 44, 1552–1562 (2014). [PubMed: 24470107]
44. Riley JS & Tait SW Mitochondrial DNA in inflammation and immunity. EMBO Rep 21, e49799 (2020). [PubMed: 32202065]
45. Miller KN et al. Cytoplasmic DNA: sources, sensing, and role in aging and disease. Cell 184, 5506–5526 (2021). [PubMed: 34715021]
46. Zhang H, Puleston DJ & Simon AK Autophagy and Immune Senescence. Trends Mol Med 22, 671–686 (2016). [PubMed: 27395769]
47. Cuervo AM & Macian F Autophagy and the immune function in aging. Curr Opin Immunol 29, 97–104 (2014). [PubMed: 24929664]
48. Phadwal K. et al. A novel method for autophagy detection in primary cells: impaired levels of macroautophagy in immunosenescent T cells. Autophagy 8, 677–689 (2012). [PubMed: 22302009]
49. Raz Y. et al. Activation-Induced Autophagy Is Preserved in CD4+ T-Cells in Familial Longevity. J Gerontol A Biol Sci Med Sci 72, 1201–1206 (2017). [PubMed: 28486590]
50. Alpert A. et al. A clinically meaningful metric of immune age derived from high-dimensional longitudinal monitoring. Nat Med 25, 487–495 (2019). [PubMed: 30842675]
51. Henson SM et al. p38 signaling inhibits mTORC1-independent autophagy in senescent human CD8(+) T cells. J Clin Invest 124, 4004–4016 (2014). [PubMed: 25083993]
52. Macian F. Autophagy in T Cell Function and Aging. Front Cell Dev Biol 7, 213 (2019). [PubMed: 31632966]
53. Wu T. et al. The TCF1-Bcl6 axis counteracts type I interferon to repress exhaustion and maintain T cell stemness. Sci Immunol 1,ea ai8593 (2016).
54. Han S, Georgiev P, Ringel AE, Sharpe AH & Haigis MC Age-associated remodeling of T cell immunity and metabolism. Cell Metab. 35, 36–55 (2023). [PubMed: 36473467]
55. Palmer DC et al. Internal checkpoint regulates T cell neoantigen reactivity and susceptibility to PD1 blockade. Med. 3, 682–704.e8 (2022). [PubMed: 36007524]
56. Neelapu SS et al. Chimeric antigen receptor T-cell therapy - assessment and management of toxicities. Nat Rev Clin Oncol 15, 47–62 (2018). [PubMed: 28925994]
57. Waldman AD, Fritz JM & Lenardo MJ A guide to cancer immunotherapy: from T cell basic science to clinical practice. Nat Rev Immunol 20, 651–668 (2020). [PubMed: 32433532]
58. Mantovani A, Allavena P, Sica A & Balkwill F Cancer-related inflammation. Nature 454, 436–444 (2008). [PubMed: 18650914]
59. Arthofer E. et al. Genetic editing of CISH enhances T cell effector programs independently of immune checkpoint cell surface ligand expression. bioRxiv, 2021.2008.2017.456714 (2021).
60. Baixauli F. et al. Mitochondrial Respiration Controls Lysosomal Function during Inflammatory T Cell Responses. Cell Metab 22, 485–498 (2015). [PubMed: 26299452]
61. Pence BD et al. Relationship between systemic inflammation and delayed-type hypersensitivity response to Candida antigen in older adults. PLoS One 7, e36403 (2012). [PubMed: 22567155]
62. Watanabe R. et al. Pyruvate controls the checkpoint inhibitor PD-L1 and suppresses T cell immunity. J Clin Invest 127, 2725–2738 (2017). [PubMed: 28604383]
63. Teijaro JR et al. Persistent LCMV infection is controlled by blockade of type I interferon signaling. Science 340, 207–211 (2013). [PubMed: 23580529]
64. Wilson EB et al. Blockade of chronic type I interferon signaling to control persistent LCMV infection. Science 340, 202–207 (2013). [PubMed: 23580528]

65. McCausland MM & Crotty S Quantitative PCR technique for detecting lymphocytic choriomeningitis virus in vivo. J Virol Methods 147, 167–176 (2008). [PubMed: 17920702]

66. Steinke FC et al. TCF-1 and LEF-1 act upstream of Th-POK to promote the CD4(+) T cell fate and interact with Runx3 to silence Cd4 in CD8(+) T cells. Nat Immunol 15, 646–656 (2014). [PubMed: 24836425]

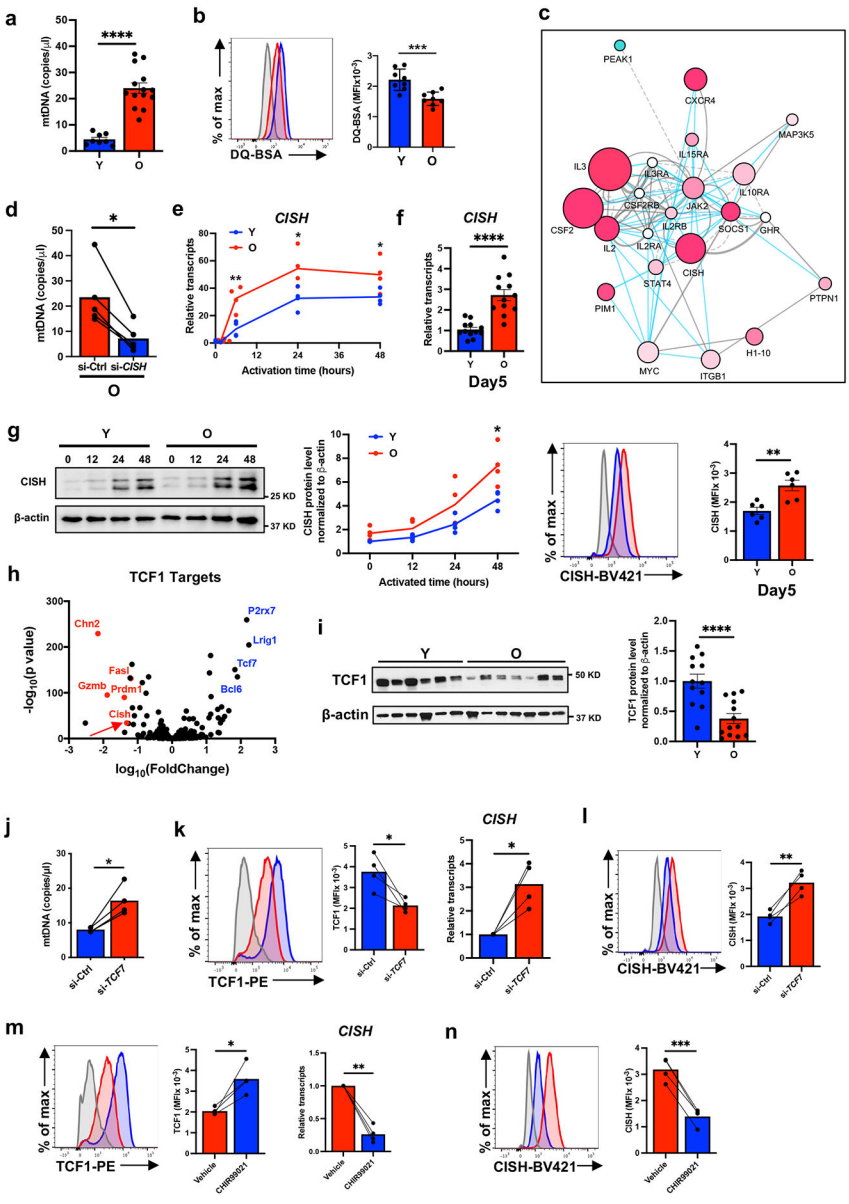

Fig. 1: Increased expression of CISH in naïve CD4$^+$ T-cell responses from older individuals.

a, mtDNA copies in supernatants of day 3-stimulated naïve CD4$^+$ T cells from eight 20 to 35 (Y) and fourteen 65 to 85-year-old (O) adults. **b**, Lysosomal proteolytic activities determined by flow cytometry of DQ-BSA-treated, day 3-stimulated naïve CD4$^+$ T cells comparing 8 young and 8 older adults. **c**, Cytoscape network of genes with differential transcript expression and chromatin accessibility comparing day 2-activated naïve CD4$^+$ T cells from young and older adults (SRA PRJNA757466). Colors indicate higher (magenta) or lower (cyan) transcripts in the old, circle sizes the number of differentially accessible sites associated with the gene. **d**, mtDNA copies in the supernatants of day 3-stimulated naïve CD4$^+$ T cells from 5 old individuals after control or *CISH* silencing. **e, f**, *CISH* transcripts from SRA PRJNA757466 at indicated time points[11] (**e**) and naïve CD4$^+$ T cells from 12 young and 12 older individuals at day 5- after stimulation (**f**). **g**, CISH protein levels at

indicated time points (left, n=4) and from day 5-stimulated naïve $CD4^+$ T cells (right, n=6) from young and older individuals. MFI, mean fluorescence intensity. **h,** Volcano plot of fold differences of TCF1 target gene expression in stem-like vs. exhausted mouse $CD8^+$ T cells from PRJNA546023[30]. TCF1 target genes were obtained from published ChIP-seq[66] (GSE52070). Comparisons by two-sided robust empirical Bayes moderated *t*-test. FC, fold change. **i,** TCF1 protein expression in day 5-stimulated naïve $CD4^+$ T cells comparing 12 young and 13 older adults. **j**, mtDNA copies in supernatants of day 3-stimulated naïve $CD4^+$ T cells from 4 young adults after control or *TCF7* silencing. **k**, **l**, TCF1 protein, *CISH* transcripts (**k**) and CISH protein (**l**) in day 3-stimulated naïve $CD4^+$ T cells from 4 young adults after *TCF7* silencing. **m**, **n**, TCF1 protein, *CISH* transcripts (**m**) and CISH protein (**n**) in day 3-stimulated naïve $CD4^+$ T cells from 4 older adults after indicated treatment. Data are presented as mean ± s.e.m. Comparison by two-tailed unpaired (a,b,e-g,i) and two-tailed paired *t* test (d,j,k-n). $*P < 0.05$, $**P < 0.01$, $***P < 0.001$, $****P < 0.0001$.

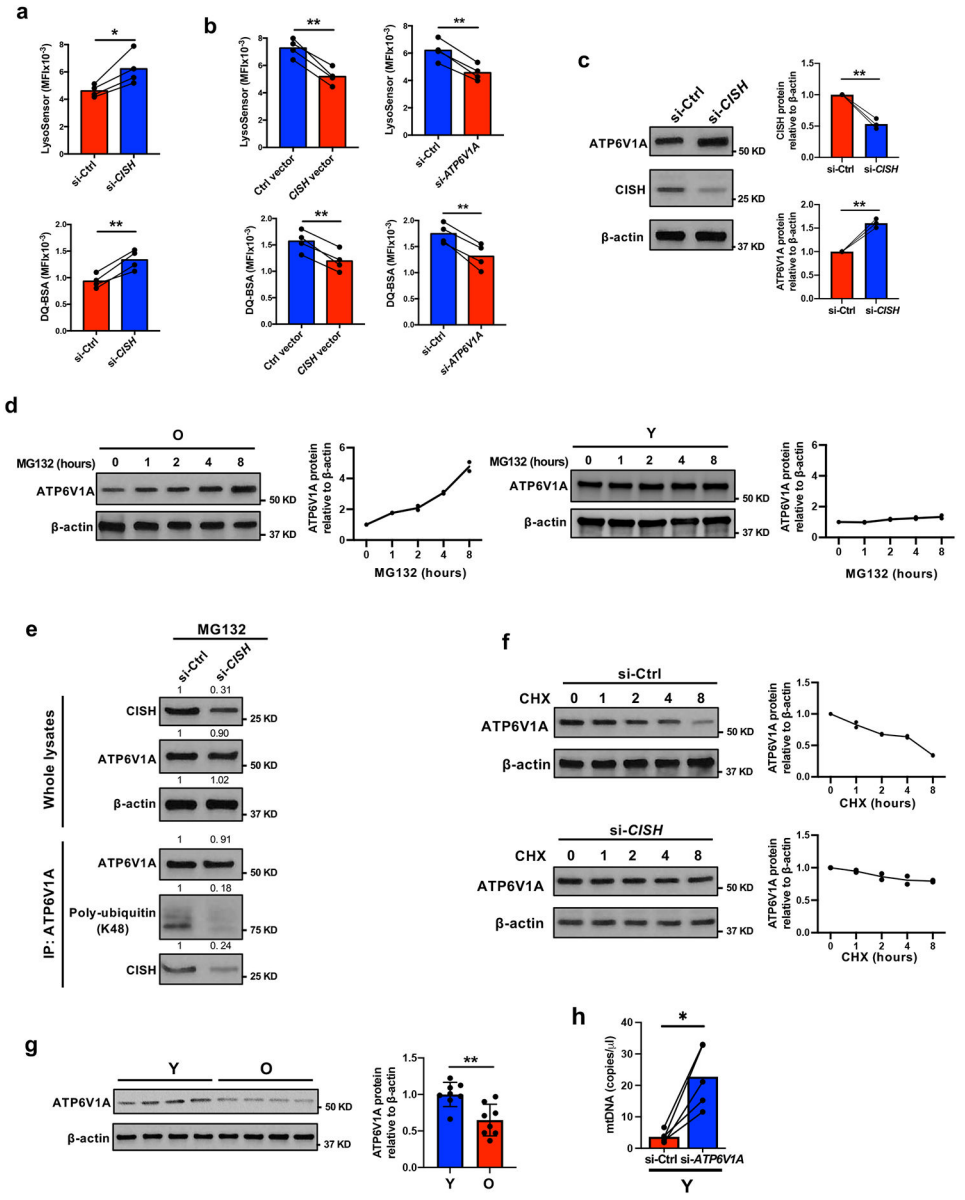

Fig. 2: CISH impairs lysosomal activity by promoting proteasomal degradation of ATP6V1A.

a, b, Naïve CD4$^+$ T cells were transfected with control, *CISH* siRNA (**a**) or *ATP6V1A* siRNA (**b**) and activated for 3 days, n=4. Alternatively, cells were transfected with pCMV6 control vector or *CISH* vector (**b**) and activated for 3 days. Lysosomal acidification (top) and proteolytic activities (bottom) were determined by flow cytometry-based analysis of LysoSensor and DQ-BSA-treated cells, respectively. **c**, Protein expression of ATP6V1A and CISH after *CISH* silencing, n=3. **d**, ATP6V1A protein expression in day 3-stimulated naïve CD4$^+$ T cells of older (left) and young (right) individuals after MG132 treatment (1 μM). **e**, Naïve CD4$^+$ T cells were transfected with control or *CISH* siRNA and activated for 3 days, the last 8 hours in the presence of 1 μM MG132. ATP6V1A was immunoprecipitated (IP). ATP6V1A and β-actin protein levels in whole-cell lysates (top). Precipitates were analyzed for ubiquitinated proteins and CISH (bottom). One representative of two experiments. **f**,

Control or *CISH*-silenced, day 3–stimulated naïve $CD4^+$ T cells were treated with CHX (5 μg/ml) to inhibit de novo ATP6V1A synthesis. Total ATP6V1A protein normalized to β-actin expression is shown relative to non-treatment. **g**, ATP6V1A protein expression of day 3-stimulated naïve $CD4^+$ T cells comparing 8 young and 8 older individuals. **h**, mtDNA copies in the supernatants of day 3-stimulated naïve $CD4^+$ T cells from 5 young after *ATP6V1A* silencing. Data are presented as mean ± s.e.m. Comparison by two-tailed paired *t* test (a-c,h) or two-tailed unpaired *t* test (g). $*P < 0.05$, $**P < 0.01$.

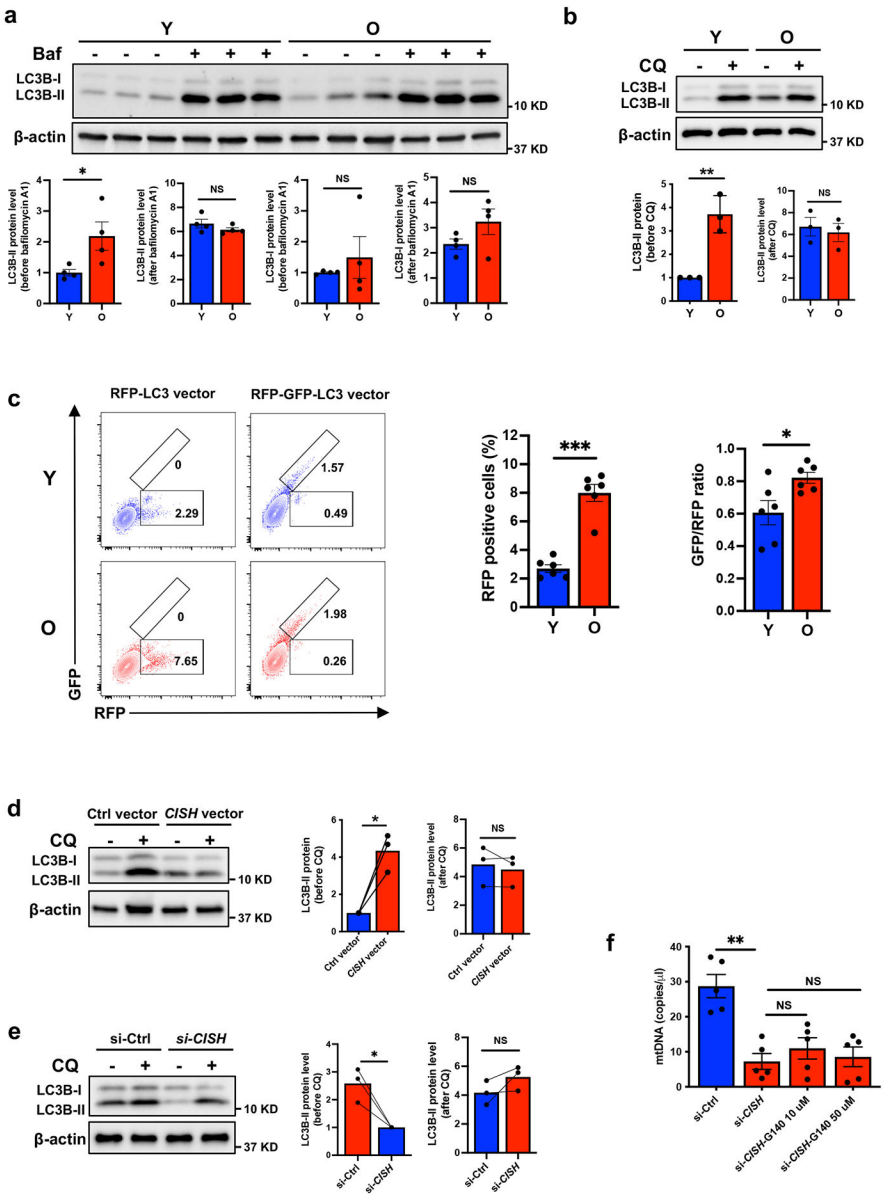

Fig. 3: CISH impairs autophagy in activated naïve CD4$^+$ T cells from older individuals.

a, Naïve CD4$^+$ T cells from young and older individuals were activated for 3 days with the last 6 hours in the presence or absence of 50 nM Bafilomycin A1 (Baf). Cells were probed for LC3B by western blotting; results for LC3B-II and LC3B-I in samples with and without Bafilomycin A1 treatment are shown, n=4. **b**, Naïve CD4$^+$ T cells from 3 young and 3 older individuals were activated for 3 days, the last 6 hours in the presence or absence of 10 μM chloroquine (CQ). Cells were probed for LC3B by immunoblotting; intensities for LC3B-II and L3B-I are shown. **c**, Naïve CD4$^+$ T cells were lentivirally transduced with an RFP-LC3 or RFP-GFP-LC3 vector. Frequencies of RFP$^+$ in RFP-LC3 and GFP$^+$RFP$^+$ in RFP-GFP-LC3 transduced day 3-stimulated naïve CD4$^+$ T cells from 6 young and 6 older individuals. Autophagic flux was determined as GFP/RFP ratio. **d, e**, Naïve CD4$^+$ T cells were transfected with pCMV6 control or *CISH*-expressing vector (**d**) or control or

CISH siRNA (**e**) and stimulated for 3 days, the last 6 hours in the presence or absence of 10 μM CQ. LC3B was immunoblotted, n=3. **f**, mtDNA copies in the supernatants of day 3-stimulated naïve $CD4^+$ T cells from 5 older individuals after *CISH* silencing plus/minus treatment with the cGAS inhibitor G140 at indicated concentrations. Data are presented as mean ± s.e.m. Comparison by two-tailed unpaired *t* test (a-c), two-tailed paired *t* test (d,e) and one-way ANOVA followed by Tukey's multiple comparisons test (f). $*P < 0.05$, $**P < 0.01$, $***P < 0.001$, and NS, not significant.

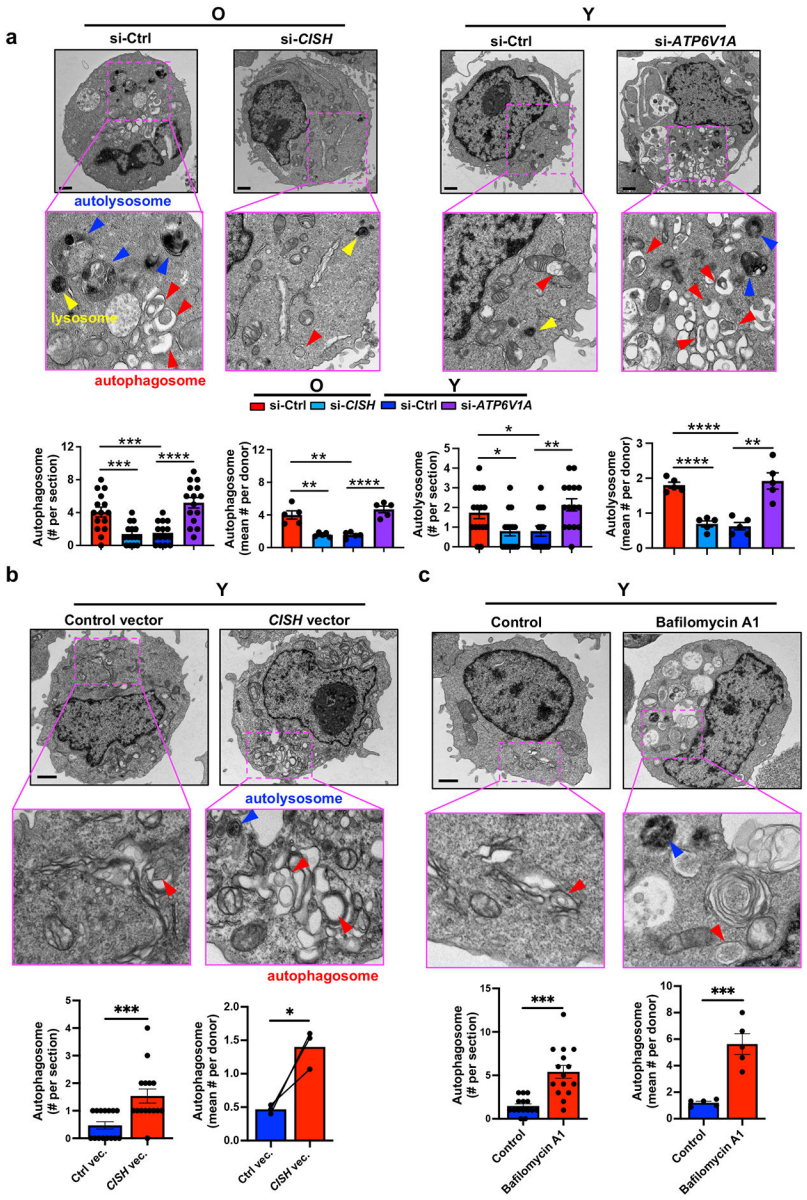

Fig. 4: CISH impairs the clearance of autophagosomes and autolysosomes.

a, Representative transmission electron microscope (TEM) images (top) and quantitative assessments of autophagosome and autolysosome numbers (bottom) in day 3-activated naïve $CD4^+$ T cells from 5 young and 5 old individuals. CISH was silenced in cells from old participants, ATP6VA1 was silenced in cells from young individuals. Image acquisition and analysis were performed by an examiner blinded to the nature of the specimen. Results from 15 sections of a representative old and young individual (left) and mean organelle numbers for each of the donors (right) are shown. **b**, Representative TEM images (top) and quantification (bottom) of autophagosome numbers in day 3-stimulated 3 young naïve $CD4^+$ T cells transfected with pCMV6 control or *CISH*-expressing vector. **c**, Representative TEM images (top) and quantitative assessments (bottom) of autophagosome number in day 3-stimulated 5 young naïve $CD4^+$ T cells cultured in the presence or absence of 5 nM

Bafilomycin A1. Scale bar, 1 μm. Data are presented as mean ± s.e.m. Comparison by two-tailed unpaired *t* test (a-c) and two-tailed paired *t* test (b). *$P < 0.05$, **$P < 0.01$, ***$P < 0.001$, and ****$P < 0.0001$.

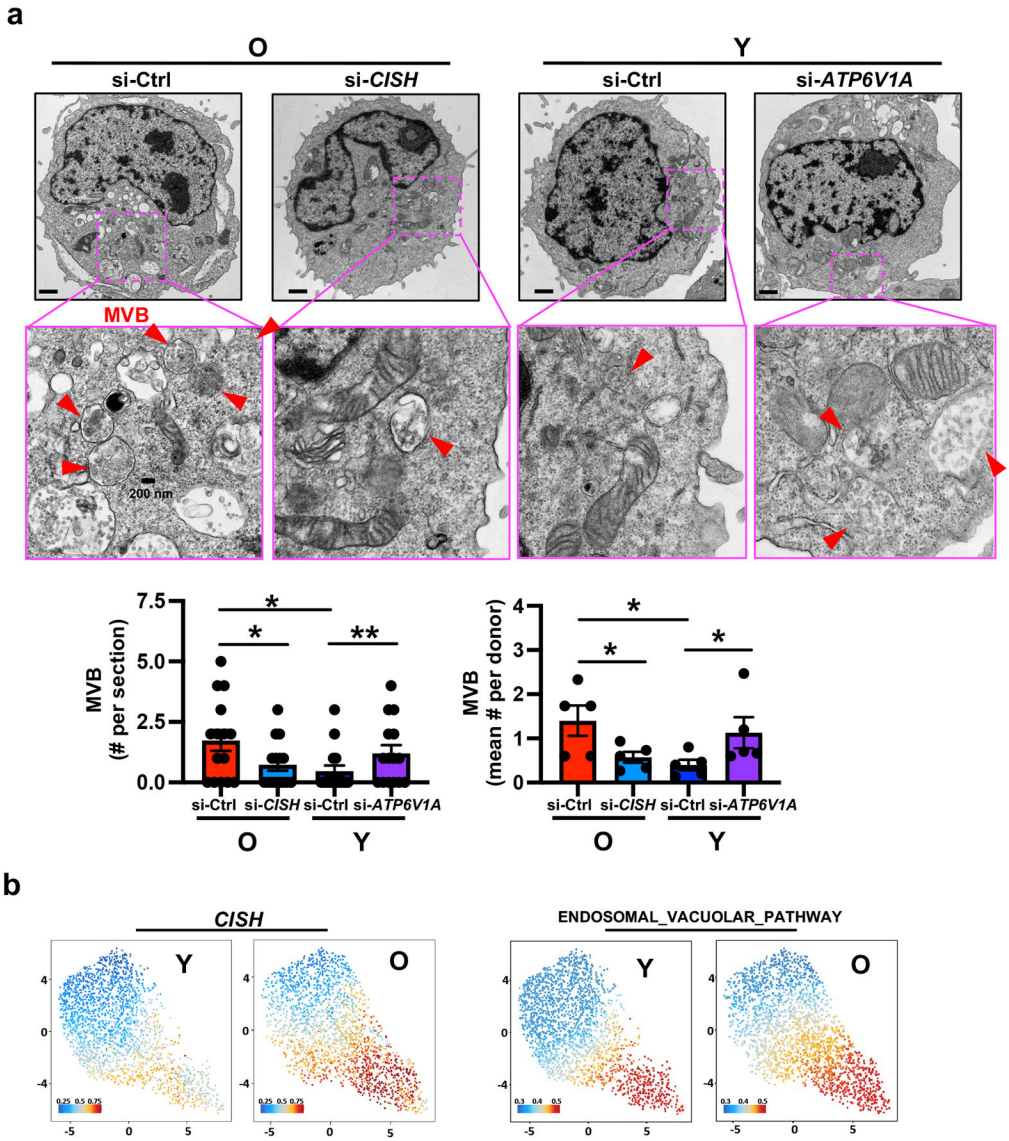

Fig. 5: CISH induces MVB expansion in naïve CD4$^+$ T cell responses from older individuals.

a, Representative TEM images (top) and quantification of MVB numbers (bottom) in day 3-activated naïve CD4$^+$ T cells from 5 young and 5 older individuals after indicated gene silencing. Data collection and analysis were conducted in a blinded manner. 15 sections were analyzed for each donor. Results from a representative old and young donor (left) and mean numbers of 5 old and 5 young donors (right) are shown. Scale bar, 1 μm. Comparison by one-way ANOVA followed by Tukey's multiple comparison test. *$P < 0.05$, **$P < 0.01$. Data are presented as mean ± s.e.m. **b**, UMAPs of integrated scATAC-seq and scRNA-seq data from activated naïve CD4$^+$ T cells from young and older adults. *CISH* transcriptional expression and enrichment scores for the ENDOSOMAL_VACUOLAR_PATHWAY module are shown by gradient color. Data are reanalyzed from elsewhere[11] under accession no. PRJNA757466.

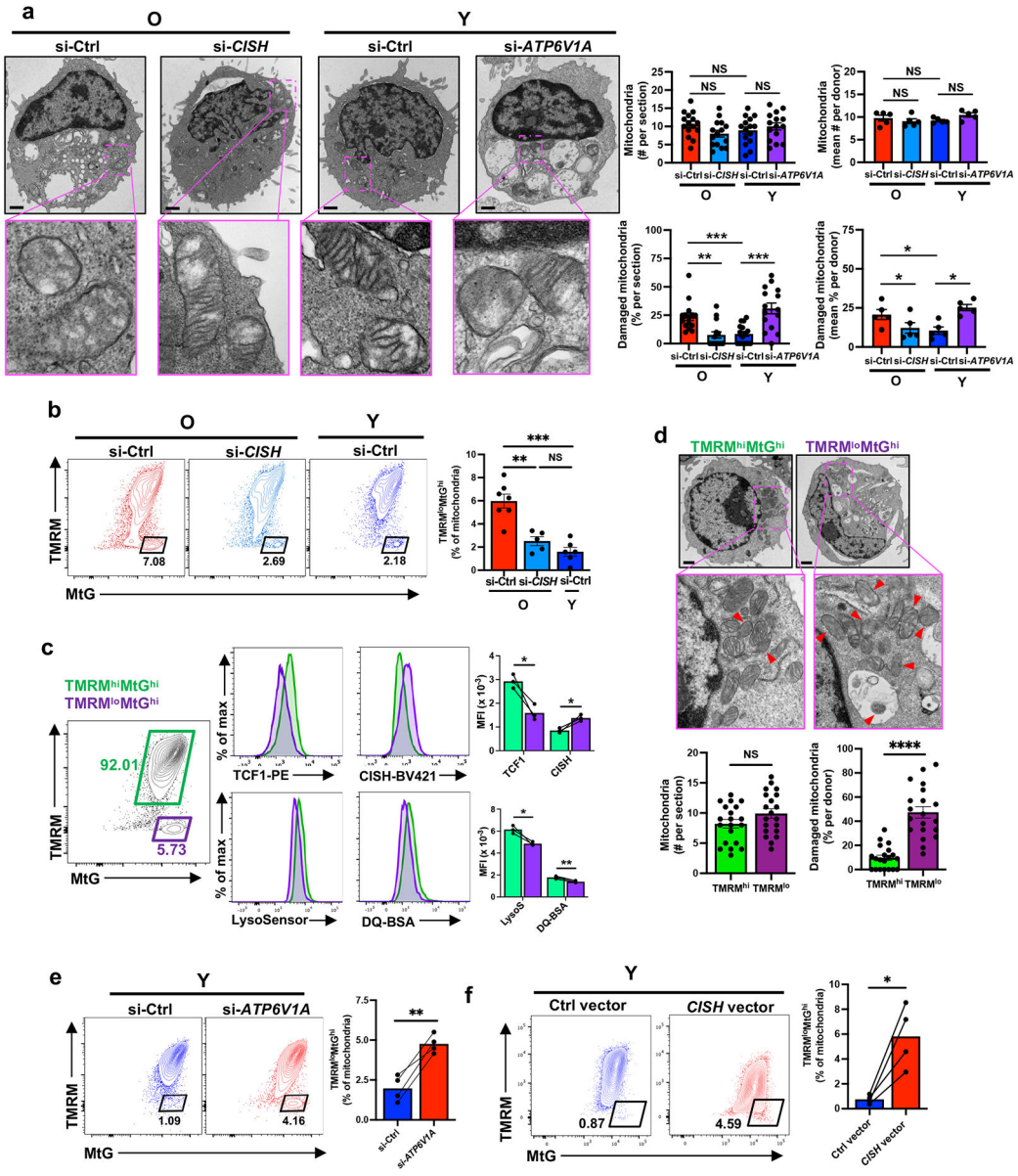

Fig. 6: CISH impairs clearance of damaged mitochondria.

a, Representative TEM images (left) and quantitative plots of total mitochondrial numbers (top) and percentage (bottom) of damaged mitochondria (right) in day 3-activated naïve $CD4^+$ T cells from 5 young and 5 older individuals after indicated gene silencing. Damaged mitochondria were determined as either no visible cristae, surrounded by a phagophore or located inside an autophagic vacuole. Data collection and analysis were conducted in a blinded manner. Results are shown for sections of representative donors and mean of 15 sections from each donor. Scale bar, 1 μm. **b**, Frequencies of $TMRM^{lo}MtG^{hi}$ population in day 3-activated naïve $CD4^+$ T cells from 6 young and 7 older individuals after *CISH* silencing. **c**, **d,** Mitochondrial mass and membrane potential of day 3-activated naïve $CD4^+$ T cells from 3 older individuals were examined using MtG (100 nM) and TMRM (10 nM), respectively. $TMRM^{hi}MtG^{hi}$ and $TMRM^{lo}MtG^{hi}$ population were sorted and analyzed for

indicated markers (**c**). Alternatively, cells were analyzed by TEM (**d**). Data collection and analysis were conducted in a blinded manner. 20 sections were analyzed for each sample. Scale bar, 1 μm. **e,** Frequencies of $TMRM^{lo}MtG^{hi}$ population in day 3-activated naïve $CD4^+$ T cells from 4 young individuals after *ATP6V1A* silencing. **f**, Frequencies of $TMRM^{lo}MtG^{hi}$ population in day 3-activated naïve $CD4^+$ T cells from 4 young individuals transfected with pCMV6 control vector or *CISH*-expressing vector. Data are presented as mean ± s.e.m. Comparison by one-way ANOVA followed by Tukey's multiple comparison test (a,b), two-tailed unpaired *t* test (d) or two-tailed paired *t* test (c,e,f). $*P < 0.05$, $**P < 0.01$, $***P < 0.001$, and $****P < 0.0001$; NS, not significant.

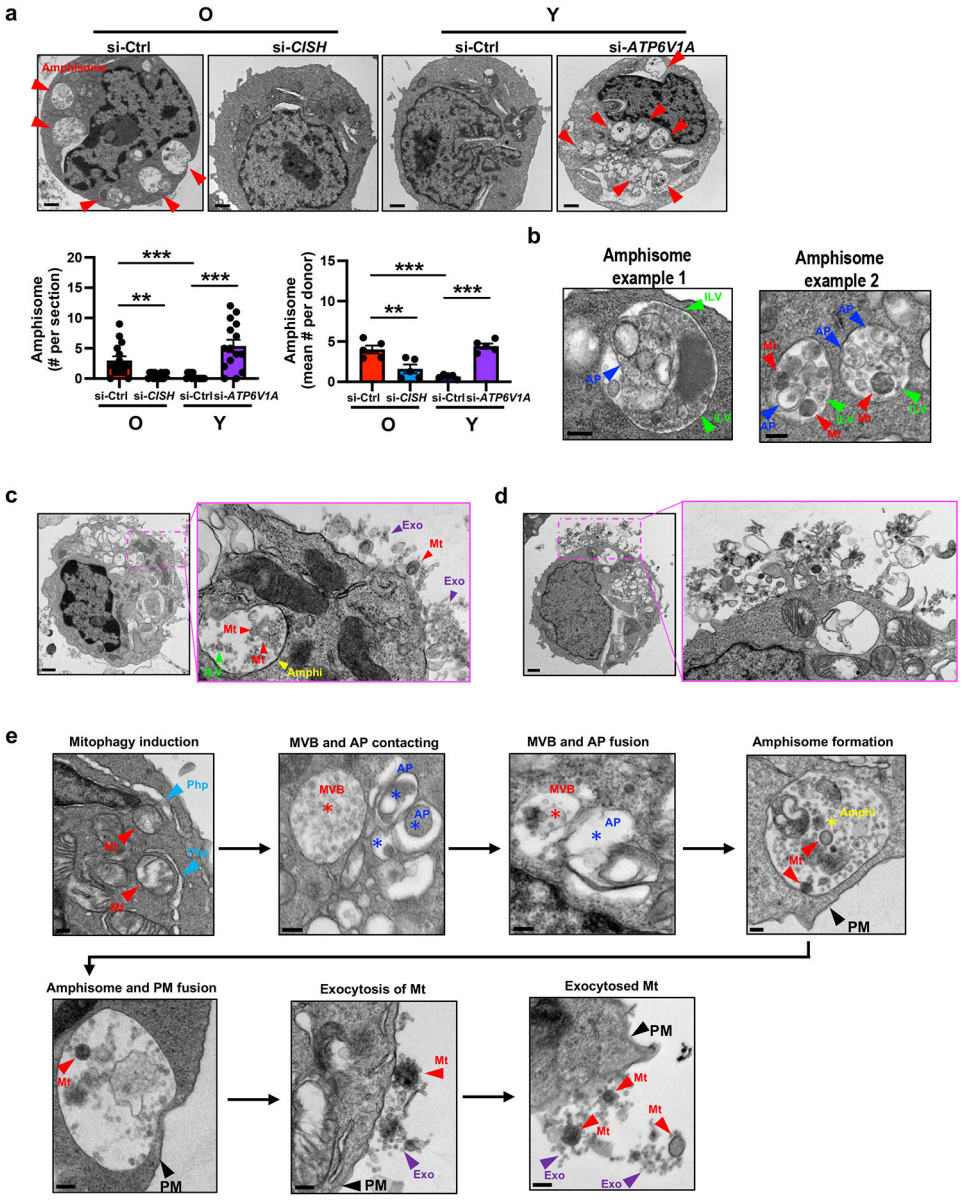

Fig. 7: CISH promotes amphisomal exocytosis of mitochondria into the extracellular environment.

a, Representative TEM images (top) and quantitative plots of amphisome numbers (bottom) in day 3-activated naïve CD4$^+$ T cells from 5 young and 5 older individuals after indicated gene silencing. Image acquisition and analysis were conducted blinded to the nature of the specimen. Results are shown for 15 sections from representative donors (left) and means of 15 sections (right) for each donor. Scale bar, 1 μm. **b**, Representative TEM images of amphisomes in day 3-activated naïve CD4$^+$ T cells from an older individual. Scale bar, 200 nm. **c**, Representative TEM image showing an intracellular amphisome containing damaged mitochondria and ILVs in a day 3-stimulated naïve CD4$^+$ T cell from an older individual and extracellular damaged mitochondria and exosomes next to the cell. Scale bar, 1 μm. **d**, Representative TEM) image showing release of cargo by a day 3-stimulated naïve CD4$^+$ T cell from an older individual. Scale bar, 1 μm. **e**, Proposed

longitudinal time course of amphisomal exocytosis as reconstructed from cross-sectional TEM images of day 3-activated naïve $CD4^+$ T cells from an older individuals. Images in c-e are representative images from the experiments described in a. Scale bar, 200 nm. Mt, mitochondria; Exo, exosome; Amphi, amphisome; PM, Plasma Membrane; AP, autophagosome; Php, Phagophore. Data are presented as mean ± s.e.m. Comparison by one-way ANOVA followed by Tukey's multiple comparison test (a). *$P < 0.05$, **$P < 0.01$, ***$P < 0.001$, and ****$P < 0.0001$.

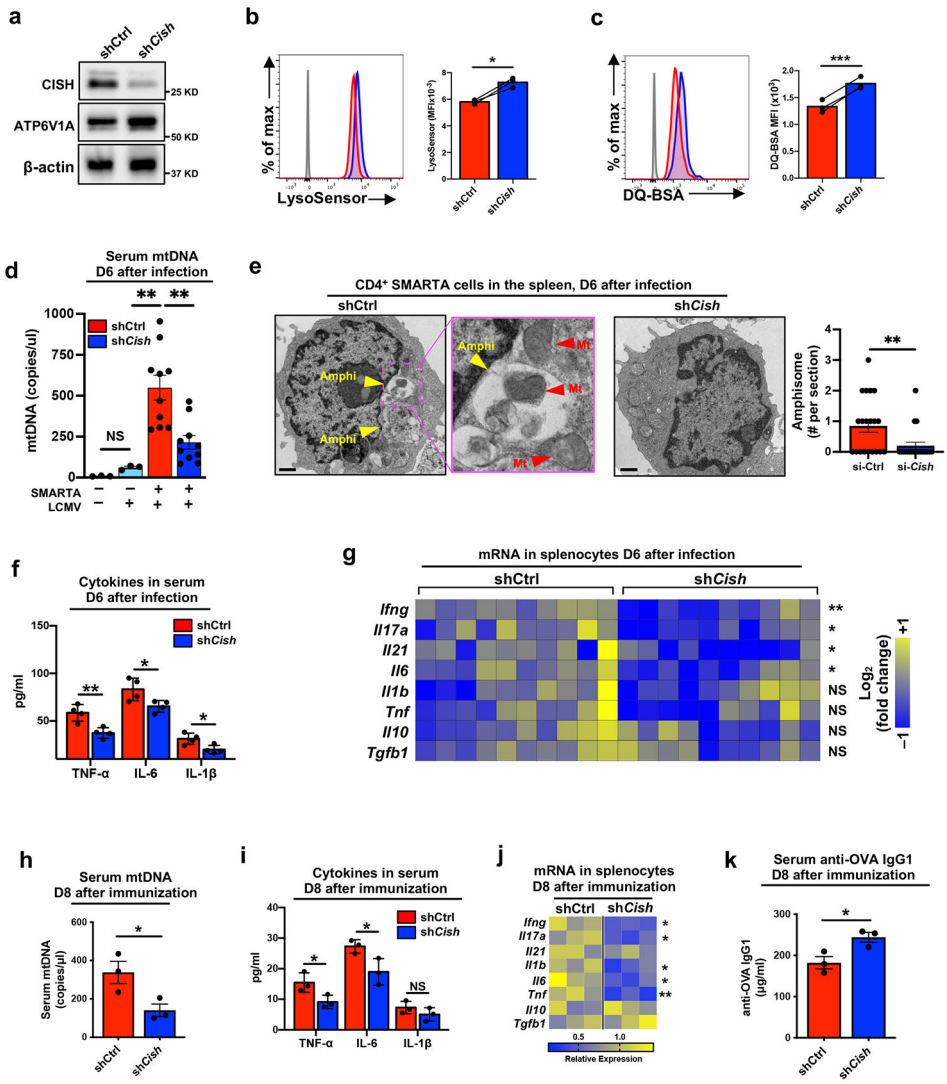

Fig. 8: *Cish* silencing attenuates mtDNA-induced inflammation in T cell responses in vivo.

a-g, sh*Cish* or shCtrl retrovirally transduced SMARTA CD4$^+$ T cells were adoptively transferred into B6 mice followed by LCMV infection. Results are pooled from three experiments with four to ten mice in each group. **a**, CISH and ATP6V1A protein expression in transduced cells before adoptive transfer. **b**, **c**, Lysosomal acidification (**b**) and proteolytic activities (**c**) in transduced cells before adoptive transfer. **d**, Serum mtDNA copies at day 6 after infection. **e**, Number of amphisomes in sorted SMARTA cells at day 6 after infection. Image acquisition and analysis were conducted in a blinded manner. Representative images and results from 20 sections for each sample. Scale bar, 1 μm. **f**, Proinflammatory cytokine concentrations in serum. **g**, Cytokine transcripts in splenocytes at day 6 after infection. **h-k**, sh*Cish* or shCtrl retrovirally transduced naïve OT-II CD4$^+$ T cells were adoptively transferred into naïve recipient followed by OVA immunization. Serum mtDNA copies (**h**), proinflammatory serum cytokine concentrations (**i**), transcripts in splenocytes (**j**) and serum anti-OVA IgG1 levels (**k**) at day 8 after immunization. Data are representative of two independent experiments with three mice per group. Data are presented as mean ± s.e.m.

Comparison by two-tailed paired *t* test (b and c), one-way ANOVA followed by Tukey's multiple comparison test (d,g,j) or two-tailed unpaired *t* test (e,f,h,i,k). $*P < 0.05$, $**P < 0.01$ and $***P < 0.001$; NS, not significant.

Table 1.

Oligonucleotide primer sets used in this study.

Name	Sequence
Ifng-F	ACAGCAAGGCGAAAAAGGATG
Ifng-R	TGGTGGACCACTCGGATGA
Il17a-F	TTTAACTCCCTTGGCGCAAAA
Il17a-R	CTTTCCCTCCGCATTGACAC
Il21-F	GGGGACAGTGGCCCATAAATC
Il21-R	GTGCCCCTTTACATCTTGTGG
Il1b-F	GAAATGCCACCTTTTGACAGTG
Il1b-R	TGGATGCTCTCATCAGGACAG
Il6-F	CTGCAAGAGACTTCCATCCAG
Il6-R	AGTGGTATAGACAGGTCTGTTGG
Tnf-F	CAGGCGGTGCCTATGTCTC
Tnf-R	CGATCACCCCGAAGTTCAGTAG
Il10-F	GCTCTTACTGACTGGCATGAG
Il10-R	CGCAGCTCTAGGAGCATGTG
Tgfb1-F	CCACCTGCAAGACCATCGAC
Tgfb1-R	CTGGCGAGCCTTAGTTTGGAC
CISH-F	GAACTGCCCAAGCCAGTCAT
CISH-R	GCTATGCACAGCAGATCCTCC
18S rRNA-F	CGCCGCTAGAGGTGAAATTCT
18S rRNA-R	CGAACCTCCGACTTTCGTTCT